

Article

C–H Metalation of Terpyridine Stereoisomers with Ni(II), Pd(II), and Pt(II)

Leo Payen , Lukas Kletsch , Tobias Lapić, Mathias Wickleder  and Axel Klein * 

Universität zu Köln, Mathematisch-Naturwissenschaftliche Fakultät, Department für Chemie, Institut für Anorganische Chemie, Greinstraße 6, D-50939 Köln, Germany; lpayen@smail.uni-koeln.de (L.P.); lukas.kletsch@uni-koeln.de (L.K.); tlasic@smail.uni-koeln.de (T.L.); mathias.wickleder@uni-koeln.de (M.W.)
* Correspondence: axel.klein@uni-koeln.de; Tel.: +49-221-470-4006

Abstract: Ni(II), Pd(II), and Pt(II) complexes [M(Y-terpy)X] (X = Cl or Br) containing the tridentate N[∩]C[∩]N-cyclometalating 2,3':5',2'' and 2,2':4',2'' stereoisomers of the well-known tridentate N[∩]N[∩]N ligand 2,2':6',2''-terpyridine (terpy) were synthesised in moderate to good yields through C–H activation. For the Pt complexes, the phenyl ethynide derivatives [Pt(Y-terpy)(C≡CPh)] were also obtained under Sonogashira conditions. In contrast to this, C[∩]N[∩]N cyclometalated complexes using the 2,2':6',3''- and 2,2':6',4''-terpy isomers were not obtained. Comparison of the N[∩]C[∩]N complexes of the cyclometalated 2,3':5',2''- and 2,2':4',2''-terpy ligands with complexes [M(dpb)Cl] of the prototypical N[∩]C[∩]N cyclometalating ligand dpb[−] (Hdpb = 2,6-diphenyl-pyridine) showed higher potentials for the terpy complexes for the ligand-centred reductions in line with the superior π-accepting properties of the terpy ligands compared with dpb. Metal-centred oxidations were facilitated by the dpb ligand carrying a central σ-donating phenyl group instead of a metalated pyridine moiety. The same trends were found for the long-wavelength absorptions and the derived electrochemical and optical band gaps. The lower σ-donating capacities of the cyclometalated terpy derivatives is also confirmed by a reduced *trans* influence in the structure of [Ni(2,3':5',2''-terpy)Br_{0.14}/OAc_{0.86}]. Attempts to re-crystallise some poorly soluble Pd(II) and Pt(II) complexes of this series under solvothermal conditions (HOAc) gave two structures with N-protonated cyclometalated pyridine moieties, [Pt(2,3':5',2''-terpyH)Cl]Cl and [Pd(2,3':5',2''-terpyH)Cl₂].

Keywords: nickel; palladium; platinum; cyclometalation; C–H activation; terpyridine



Citation: Payen, L.; Kletsch, L.; Lapić, T.; Wickleder, M.; Klein, A. C–H Metalation of Terpyridine Stereoisomers with Ni(II), Pd(II), and Pt(II). *Inorganics* **2023**, *11*, 174. <https://doi.org/10.3390/inorganics11040174>

Academic Editor: Antonino Gulino

Received: 4 April 2023
Revised: 17 April 2023
Accepted: 18 April 2023
Published: 21 April 2023

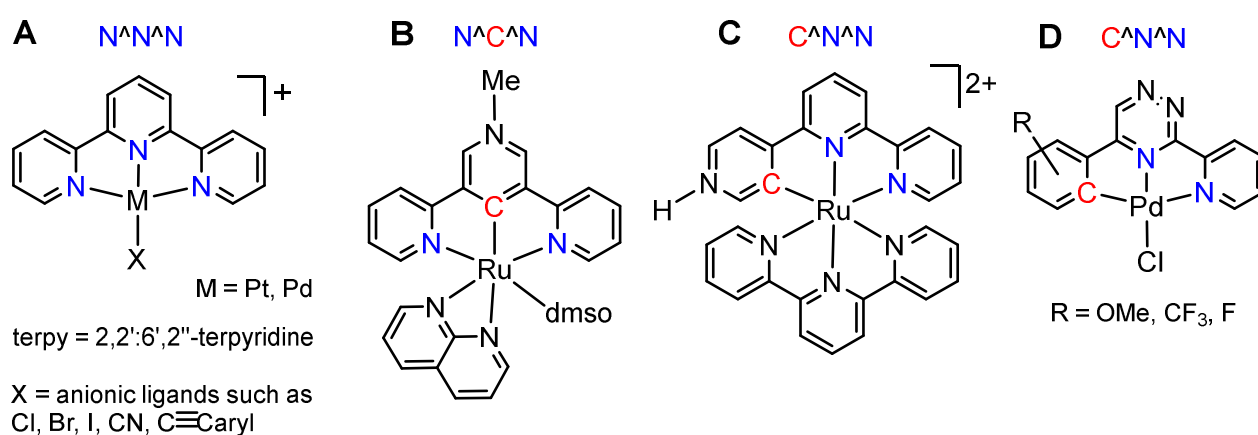


Copyright: © 2023 by the authors. Licensee MDPI, Basel, Switzerland. This article is an open access article distributed under the terms and conditions of the Creative Commons Attribution (CC BY) license (<https://creativecommons.org/licenses/by/4.0/>).

1. Introduction

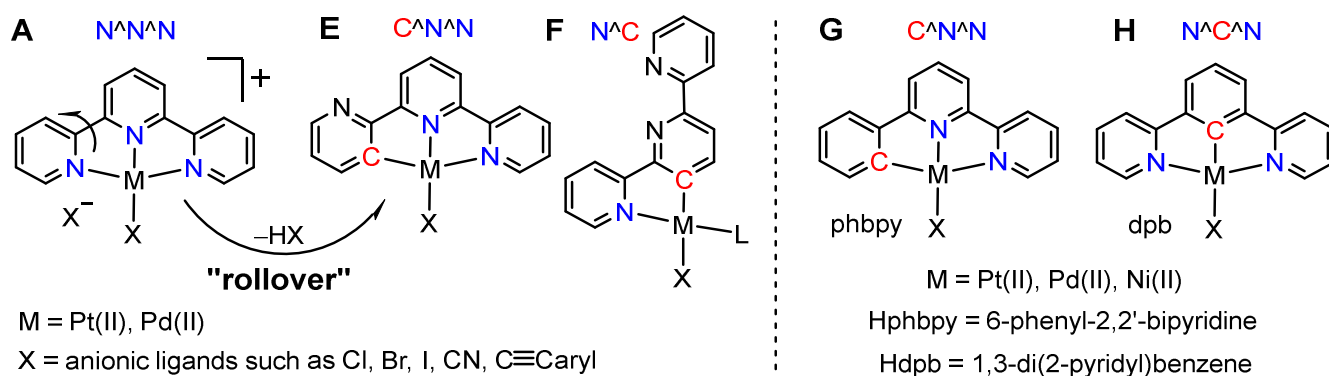
C–H activation and metalation is the starting step in transition metal-catalysed C–H functionalisation reactions [1–7]. The directing group (DG) approach shows that C–H metalation is often one of the key steps of such a reaction [1–3,5,6]. The well-known tridentate N[∩]N[∩]N-coordinating ligand 2,2':6',2''-terpyridine (terpy, Scheme 1A) and substituted derivatives have been reported in literally hundreds of Ni(II), Pd(II), or Pt(II) complexes or coordination polymers with applications in C–H or C–X functionalisation catalysis [8–12]. At the same time, they have been studied as supramolecular units [13–20], luminescent [15–23], photoreactive [21–23], or redox-active materials [10,24,25], and as biomedical probes [15–20,26].

In contrast to this, the potential cyclometalation of this ligand to transition metals has been attempted only in very few cases [27–29]. The only examples of terpy being metalated are the Ru(II) complex [Ru(MeNterpy)(napy)(dmsol)] (napy = 8-naphthyridine) containing a Me-N₄ alkylated zwitterionic MeN(+)terpy(−) N[∩]C[∩]N cyclometalated ligand [27] (Scheme 1B) and the Ru(II) complex [Ru(terpy)(terpy*)]²⁺ containing the N^{4''} protonated C[∩]N[∩]N metalated 2,2':6':4''terpy ligand (Scheme 1C) [28]. Previously, we found C[∩]N[∩]N cyclometalated dipyriddy-triazines in Pd(II) complexes [Pd(L–H)Cl] (L = 5-aryl-3-(2'-pyridyl)-1,2,4-triazine) in an EI-MS(+) experiment (Scheme 1D) but could not isolate this species [29].



Scheme 1. (A) Cationic $[M(\text{terpy})\text{Cl}]^+$ [Pt: ref. [20]; Pd: refs. [29,30]] and examples of cyclometalated terpy derivatives. (B) $[\text{Ru}(\text{MeNterpy})(\text{napy})(\text{dmsu})]$ (napy = 8-naphthyridine) ligand from ref. [27]. (C) $[\text{Ru}(\text{terpy})(\text{terpy}^*)]^{2+}$ (terpy* = $N4''$ protonated $C^{\wedge}N^{\wedge}N$ 2,2':6':4''terpy) from ref. [28]. (D) $[\text{Pd}(\text{L})\text{Cl}]$ (L = 5-aryl-3-(2'-pyridyl)-1,2,4-triazine) from ref. [29].

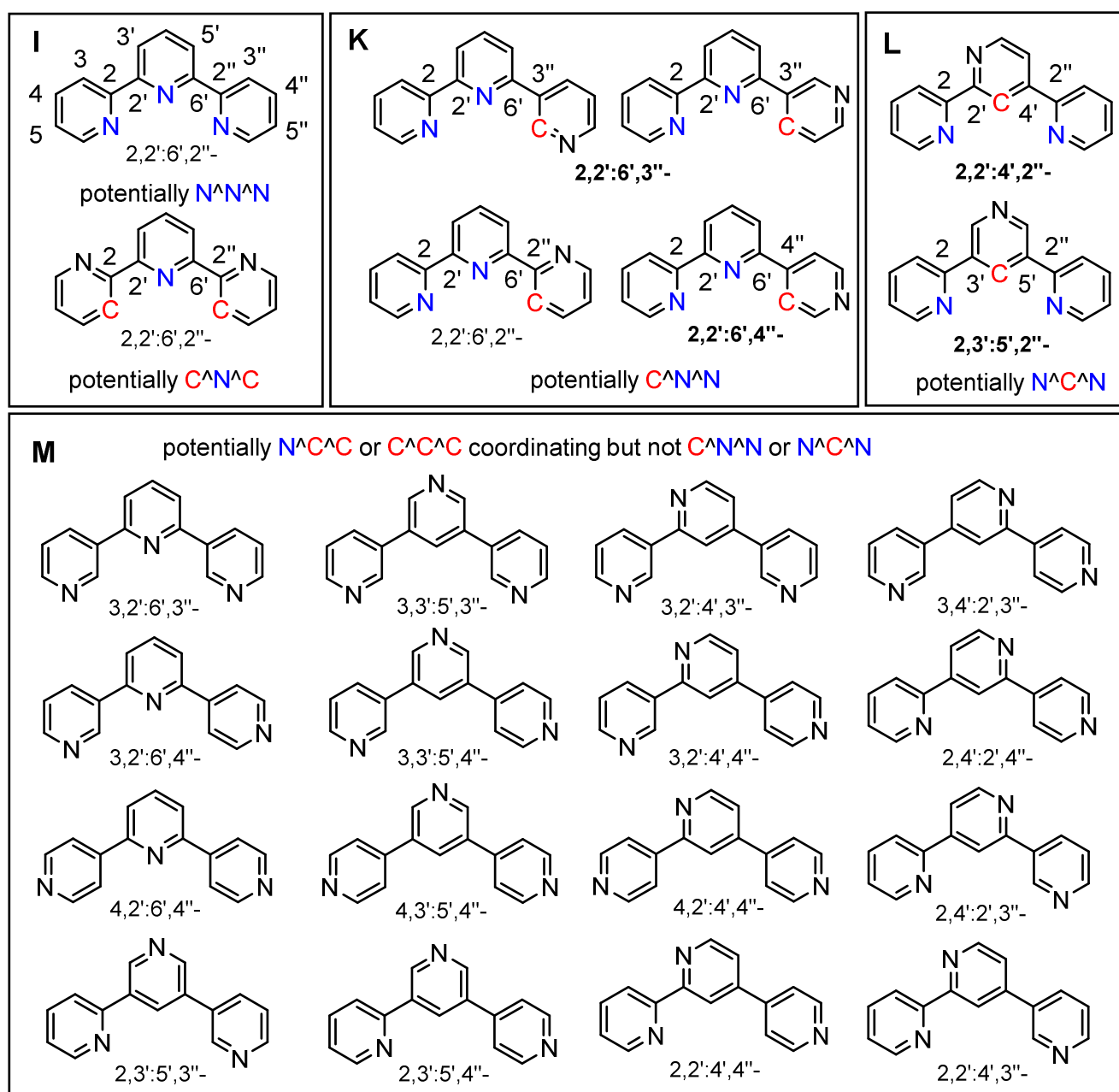
Basically, a so-called “rollover cyclometalation” starting from the $N^{\wedge}N^{\wedge}N$ -coordinated $[M(\text{terpy})\text{X}]^+$ complexes (Scheme 2A) could yield $C^{\wedge}N^{\wedge}N$ -coordinated neutral complexes $[M(\kappa^3\text{-}C^{\wedge}N^{\wedge}N\text{-terpy})\text{X}]$ (Scheme 2E). Such reactions have been intensely studied for the $N^{\wedge}N$ bidentate ligand 2,2'-bipyridine (bpy) and its derivatives with M = Pt(II), Pd(II) [4,31–34], and Ir(III) [11]. However, rollover metalation has never been observed for either terpy or bpy coordinated to Ni(II). Alternatively, a $N^{\wedge}C$ coordination in mononuclear complexes of the type $[M(\kappa^2\text{-}N^{\wedge}C\text{-terpy})\text{X}(\text{L})]$ (Scheme 2F) or dinuclear species containing a bridging $\kappa^2\text{-}C^{\wedge}N\text{-}\mu\text{-}\kappa^2\text{-}N^{\wedge}N\text{-terpy}$ ligand are possible with the terpy ligand but have also never been reported.



Scheme 2. (A) Cationic $N^{\wedge}N^{\wedge}N$ -coordinated cationic Pt(II) and Pd(II) complexes of 2,2':6':2''-terpyridine; potential (E) $C^{\wedge}N^{\wedge}N$ - or (F) $N^{\wedge}C$ -coordinated terpy derivatives in neutral M–X complexes; M–X complexes of the prototypical $C^{\wedge}N^{\wedge}N$ and $N^{\wedge}C^{\wedge}N$ coordinating ligands $^{\ominus}\text{phbpy}$ (G) and $^{\ominus}\text{dpb}$ (H).

This is remarkable in view of the broad use of the very similar $C^{\wedge}N^{\wedge}N$ or $N^{\wedge}C^{\wedge}N$ -type cyclometalating ligands $^{\ominus}\text{phbpy}$ (Hphbpy = 6-phenyl-2,2'-bipyridine, Scheme 2G) and $^{\ominus}\text{dpb}$ (dpbH = 1,3-di(2-pyridyl)benzene, Scheme 2H) in complexes of nickel group elements [4,19,21,35–53]. Pt(II) and Pd(II) complexes of these two ligands and their derivatives have been reported as efficient triplet emitters [36–45], and some Pd(II) and Ni(II) complexes have found application in catalysis [47–49,52]. Very recently, we studied complexes $[M(\text{phbpy})(\text{CN})]$ of the Ni-Pd-Pt triad with the $C^{\wedge}N^{\wedge}N$ binding $^{\ominus}\text{phbpy}$ ligand (Scheme 2G) [44] and the $N^{\wedge}C^{\wedge}N$ binding 4,6-dimethylated dpb derivative $^{\ominus}\text{Me}_2\text{dpb}$ ($[\text{M}(\text{Me}_2\text{dpb})\text{Cl}]$, Scheme 2H) [43], and found interesting electrochemical and photophysical properties through the series of varied metals.

When looking at the complete list of stereoisomers of terpy, we count 21 isomers (Scheme 3) [13,14,54,55]. The parent 2,2':6',2'' isomer is potentially able to undergo double-cyclometalation, forming a C^NC^N chelate in addition to the common N^NN^N coordination (Scheme 3I). At the same time, the parent isomer is able to undergo single cyclometalation leading to a C^NN^N coordination (Scheme 3K), which is also true for the 2,2':6',3'' and the 2,2':6',4'' isomers. The 2,2':4',2'' and the 2,2':6',4'' isomers are capable of performing cyclometalation resulting in a N^CC^N coordination (Scheme 3L).



Scheme 3. Representation of 2,2':6',2''-terpyridine (terpy) and the so-called ring-confused stereoisomers (with numbering). (I) N^NN^N and potential C^NC^N binding mode of the parent 2,2':6',2'' derivative; (K) potentially N^NC^N (C^NN^N) binding isomers; (L) potentially N^CC^N binding isomers; and (M) further isomers. The derivatives studied in this work are marked in bold in (K,L). Note that there is only one 2,2':6',3'' derivative, but this has two different options for cyclometalation.

For the further 16 terpy isomers (Scheme 3M), N[∧]C[∧]C, C[∧]N[∧]C, or C[∧]C[∧]C cyclometalations are potentially possible. Double N[∧]C[∧]C cyclometalation with dianionic N[∧]C[∧]C²⁻ ligands based on diphenyl-2-pyridine (Hdphpy) was never observed for Pt(II), while for Pd(II) and Ni(II), the complexes [M(dphpy)(PPh₃)] (M = Pd and Ni) were recently reported [56]. In contrast to this, ⁻C[∧]N[∧]C⁻ coordination with the prototypical 2,6-diphenylpyridine system (Hdpp) to Pt(II) is quite frequent [57–62], while for Pd(II) the first example was only very recently reported [Pd(dpp)(PPh₃)] [63], and no Ni(II) derivatives have been found. Triple C[∧]C[∧]C cyclometalation is not known for any of these metals.

Being interested in comparative studies of isoleptic Pt(II), Pd(II), and Ni(II) complexes [39,43,44,64,65], we started to explore the capacity of the 2,2':6',3'' and 2,2':6',4''-terpy isomers for C[∧]N[∧]N cyclometalation (Scheme 3K), as well as the capacity of the 2,2':4',2'' and 2,3':5',2'' isomers for N[∧]C[∧]N cyclometalation (Scheme 3L).

We herein report on attempts to N[∧]C[∧]N cyclometalate the 2,2':4',2'' and 2,3':5',2'' derivatives forming the chlorido complexes [M(N[∧]C[∧]N)Cl] (M = Ni, Pd, or Pt) and the derivatisation of Pt–Cl complexes into the alkynyl derivatives [Pt(N[∧]C[∧]N)(C≡CPh)] (Scheme 4N,O). We report on the details of the synthesis procedures, which were different for the chlorido Pt and Pd complexes compared with the Ni derivatives. Additionally, we studied in detail the impact of the electron-withdrawing N moieties in the cyclometalated terpy ligands on the electronics of the Pt(II), Pd(II), and Ni(II) complexes in comparison with the prototypical N[∧]C[∧]N coordinating dpb⁻ (Scheme 2H) and the C[∧]N[∧]N coordinating phbpy⁻ ligand (Scheme 2G). Comparative UV-vis absorption and electrochemical data are available for the series [M(Me₂dpb)Cl] [43], [M(dpb)Cl] [43,48–50], and [M(phbpy)X] (M = Pt, Pd, Ni, X = Cl or Br) [51,52].

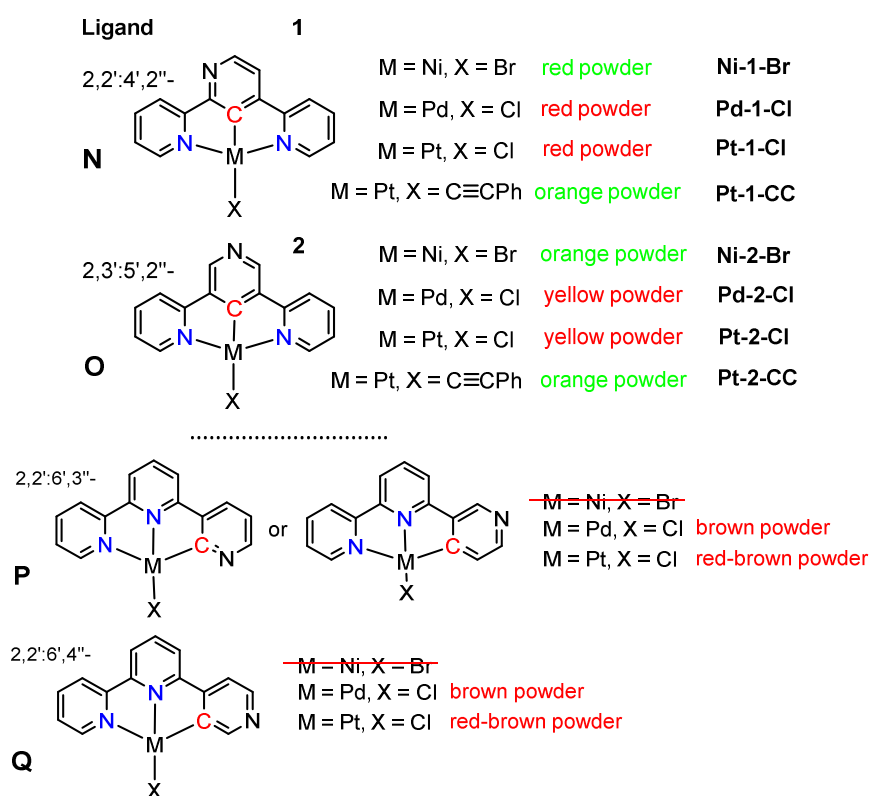
Table 1. Overview of attempted complex syntheses using 2,2':6',3''- and 2,2':6',4''-terpy ligands.

Terpy Ligand	Precursor	Conditions	Product
2,2':6',3''	NiBr ₂	KOAc/K ₂ CO ₃ , <i>p</i> -xylene, reflux, 67 h	no conversion, ligand re-isolated
2,2':6',3''	[Ni(DME)Br ₂]	NEt ₃ , THF, reflux, 16 h	no conversion, ligand re-isolated
2,2':6',4''	NiBr ₂	KOAc/K ₂ CO ₃ , <i>p</i> -xylene, reflux, 69 h	red–brown powder ^c
2,2':6',3''	K ₂ PdCl ₄	MeCN/H ₂ O, reflux, 18 h	brown powder (12%) ^a
2,2':6',4''	K ₂ PdCl ₄	MeCN/H ₂ O, reflux, 19 h	no conversion, ligand re-isolated
2,2':6',4''	K ₂ PdCl ₄	DMF, reflux, 65 h	brown powder (7%) ^{a,b}
2,2':6',3''	K ₂ PtCl ₄	Glacial HOAc, reflux, 19 h	red–brown powder (24%) ^a
2,2':6',4''	K ₂ PtCl ₄	Glacial HOAc, reflux, 67 h	red–brown powder (33%) ^a

^a Identified by (+)-HR-ESI-MS; ^b identified by (+)-HR-EI-MS; ^c decomposed under ambient conditions. KOAc = potassium acetate; DME = dimethoxy-ethane; THF = tetrahydrofuran; MeCN = acetonitrile; DMF = dimethyl formamide; HOAc = acetic acid.

Unfortunately, for the C[∧]N[∧]N cyclometalated complexes attempted from the 2,2':6',3'' and 2,2':6',4'' isomers (Scheme 4P,Q), we either did not isolate any reasonable product (M = Ni) or obtained materials which were virtually insoluble, thus massively hampering characterisation (M = Pd and Pt). We included these results for the sake of completeness and to encourage others to report negative results.

In this contribution, we discuss the successful and the failed synthesis attempts in view of the different structural patterns of the ligands. We will also try to draw conclusions for the use of cyclometalated Pt(II), Pd(II), and Ni(II) complexes of terpy derivatives in C–H functionalisation reactions as catalysts or models for catalyst intermediates.



Scheme 4. The Ni, Pd, and Pt complexes synthesised in this study. Green labels = successful synthesis and characterisation; red labels = obtained material was virtually insoluble, only partially characterised; red strike-through = no products isolated. For the complexes labelled M-L-X in (N,O), to the right, electrochemical and UV-vis absorption data were recorded. (P,Q) represent not further characterised products (see also Table 1).

2. Results and Discussion

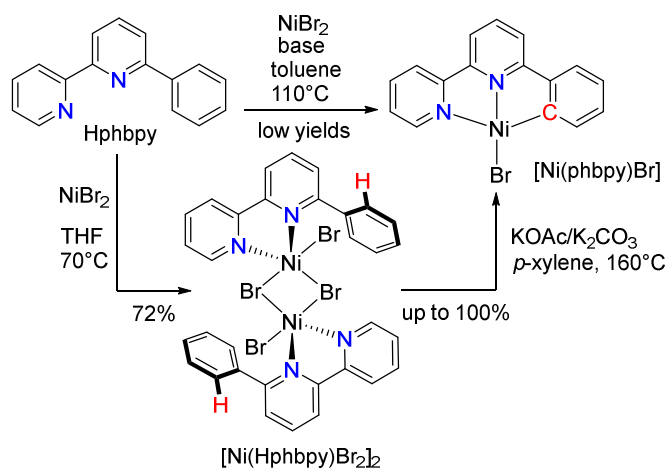
2.1. Preparation and Analytical Characterisation

The terpy stereoisomers 2,2':6',3''-terpy and 2,2':6',4''-terpy (Scheme 3K) were synthesised via modified Kröhnke synthesis [66] from 2-acetylpyridine and either 3-acetylpyridine or 4-acetylpyridine, respectively (see Supplementary Materials). 2,2':4',2''-terpy and 2,3':5',2''-terpy (Scheme 3L) were obtained from Negishi cross-couplings of 2-bromopyridine with either 3,5-dibromopyridine or 2,4-dibromopyridine, respectively. The ligands were characterised by nuclear magnetic resonance (NMR) spectroscopy (data in the Supplementary Materials).

The N[∩]C[∩]N cyclometalated Ni(II) complexes [Ni(2,3':5',2''-terpy)Br] (**Ni-1-Br**) and [Ni(2,2':4',2''-terpy)Br] (**Ni-2-Br**) were synthesised from NiBr₂ and the terpy derivatives at 60 and 55% yield, respectively, using the previously reported base-assisted C–H deprotonation/metalation method (potassium acetate (KOAc), potassium carbonate (K₂CO₃) in *p*-xylene as solvent, under reflux) [43,50]. For more details, see Section 3. The two complexes were analysed and further characterised by ¹H NMR, electrospray ionisation mass spectrometry (ESI-MS) in the positive mode (+), and electron ionisation mass spectrometry (EI-MS(+)). Recently, we obtained the N[∩]C[∩]N-coordinated complexes [Ni(Me₂dpb)Cl] (Me₂dpbH = 1,5-di(2-pyridyl)-2,4-dimethylbenzene) [43] and [Ni(dpb)X] (Hdpb = 1,3-di(2-pyridyl)-benzene, X = Cl, Br, I) [50] using the same base-assisted C–H activation method (KOAc/K₂CO₃, *p*-xylene), and obtained excellent (94%, Me₂dpb) or good (73–81%, dpb) yields. The success in metalating the 2,3':5',2'' and 2,2':4',2''-terpy derivatives underlines the versatility of this method.

Attempts to react NiBr₂ in the same way with the potentially C[∩]N[∩] coordinating 2,2':6',3''-terpy and 2,2':6',4''-terpy led to orange–red solutions from which we could not

isolate any material with the expected elemental composition, NMR spectrum, or MS pattern. Further attempts using $[\text{Ni}(\text{DMF})\text{Br}_2]$ as precursor also failed (more details in the Materials and Methods section). This is remarkable as we previously reacted the protoligand Hphbpy (Scheme 2G) with NiBr_2 in the same way and obtained $[\text{Ni}(\text{phbpy})\text{Br}]$ with excellent yield [51]. In this previous study, we also showed that the N^N pre-coordination of Hphbpy plays an important role in the cyclometalation reaction (Scheme 5).



Scheme 5. Cyclonickelation of Hphbpy to $[\text{Ni}(\text{phbpy})\text{Br}]$ and efficient pre-coordination forming $[\text{Ni}(\text{Hphbpy})\text{Br}_2]_2$. From ref. [51].

For both 2,2':6',3''- and 2,2':6',4''-terpy isomers, such a pre-coordination is possible. However, no such species were observed by either colour change of the reaction mixture or formation of precipitates. Slight colour changes towards a red colour typically associated with Ni-phbpy-type complexes were observed; however, for both ligands, no complexes were isolated. Either we did not achieve any conversion or the isolated crude product decomposed under ambient conditions (Table 1).

When compared with the prototypical Hphbpy ligand, the failure to cyclonickelate these terpy ligands cannot lie in the electron deficiency of the pending 2-, 3-, or 4-pyridyl groups compared with the phenyl group in Hphbpy because the lower electron density of a pyridine should facilitate rather than hamper proton abstraction. Thus, we assume that the rollover nickelation of these pyridyl groups is hampered (Scheme 2). Future quantum chemical calculations will seek to gain insight into the details, especially the energetics of the assumed reaction mechanism.

Synthesis of the N^C^N-coordinated Pd(II) complexes of the 2,2':4',2''- and 2,3':5',2''-terpy ligands was attempted using a method established for the cyclometalation of Hphbpy [67]. Reacting $\text{K}_2[\text{PdCl}_4]$ and the terpy derivatives in $\text{MeCN}/\text{H}_2\text{O}$ [67] allowed $[\text{Pd}(2,2':4',2''\text{-terpy})\text{Cl}]$ (**Pd-1-Cl**) to be obtained as a red powder and $[\text{Pd}(2,3':5',2''\text{-terpy})\text{Cl}]$ (**Pd-2-Cl**) to be obtained as a yellow powder with isolated yields of 84% and 57%, respectively. The products were characterised by high-resolution electrospray ionisation mass spectrometry (HR-ESI-MS), UV-vis absorption spectroscopy, and cyclic voltammetry, while NMR spectroscopic characterisation was prevented by very low solubility. Even measurements in hot (40°C) deuterated dimethylsulfoxide ($\text{DMSO}-d_6$), recorded on the 600 MHz NMR instrument using 256 scans, did not provide any meaningful signals. We tried to re-crystallise the powders using solvothermal methods to receive single crystals for X-ray diffraction but failed to do so. Instead, we obtained the crystal structure of the complex $[\text{Pd}(2,3':5',2''\text{-terpyH})\text{Cl}_2]$ (**Pd-H2-Cl₂**), featuring a bidentate C^N cyclometalation of the central pyridine ring and a N-H protonation close to the metalated C atom (see later for structure details) instead of the desired N^C^N-type coordination. This product was likely formed under the solvothermal conditions applied for crystallisation, since no traces of this species were found in any of the other analytical methods used for characterisation.

Attempts to react $K_2[PdCl_4]$ in the same way with the potentially C[∞]N[∞] coordinating 2,2':6',3''-terpy and 2,2':6',4''-terpy led to the isolation of brown powders at 12% and 7% yield after the typical workup. Virtual insolubility prevented any characterisation in solution, and the formation of the desired compounds was thus only confirmed in HR-ESI-MS experiments. Further attempts using Pd(OAc)₂ or [Pd(COD)Br₂] (COD = 1,5-cyclooctadiene) as Pd precursors, using either acidic conditions (HOAc or trifluoromethyl acetic acid) or the addition of bases such as NEt₃ or *n*-BuLi, were not successful (Table 1).

We recently found that [Pd(terpy)Cl]Cl (C₁₅H₁₁N₃PdCl₂) showed EI-MS(+) signals at $m/z = 375$, indicating the cyclometalated species [Pd(terpy-H)Cl]⁺ (C₁₅H₁₀N₃PdCl) formed under the harsh conditions of the MS experiment [29]. However, attempts to produce a cyclometalated complex starting from [Pd(terpy)Cl]Cl in a chemical reaction failed [29]. This is fully in line with the herein reported difficulties in obtaining a Pd(C[∞]N[∞]) coordination through rollover palladation.

The Pt(II) N[∞]C[∞]N complexes [Pt(2,2':4',2''-terpy)Cl] (**Pt-1-Cl**) and [Pt(2,3':5',2''-terpy)Cl] (**Pt-2-Cl**) were obtained as red (2,2':6',4'', 40% yield) or yellow (2,3':5',2'', 63% yield) powders, respectively, using an established method by heating $K_2[PtCl_4]$ and the terpy derivatives in glacial HOAc [46]. The products were characterised by HR-ESI-MS, UV-vis absorption spectroscopy, and cyclic voltammetry, while NMR spectroscopy was prevented by very poor solubility. We obtained single crystals of the compound [Pt(2,3':5',2''-terpyH)Cl]·Cl (**Pt-H2-ClCl**) by heating the yellow product in a glass ampule containing acetic acid under solvothermal conditions.

The same reaction protocol applied to the potentially C[∞]N[∞] coordinating 2,2':6',3''- and 2,2':6',4''-terpy derivatives led to the isolation of red-brown powders at 24% and 33% yield after the typical workup. These materials are completely insoluble, which prevented any characterisation (Table 1). For comparison, synthesis of the prototypical C[∞]N[∞]-coordinated complexes [M(phbpy)X] (Hphbpy = 6-phenyl-2,2'-bipyridine, Scheme 2G) has previously been achieved using several methods, including base-assisted C-H activation (M = Ni, Pd), [43,50] other base-assisted methods (Ni) [53], the boiling HOAc method (Pt, Pd) [48,49], and milder electrophilic substitution reactions such as reactions in MeCN/H₂O mixtures (Pd) [67], starting from various metal precursors. At the moment, we are not sure if the isolated materials correspond to the targeted complexes or were just decomposition products. In a future study, we will use substituted ligand derivatives to render potential products more soluble. On the other hand, the low yields and comparison with the results from the reactions with Pd(II) let us suspect that our attempts to obtain cyclometalated Pt(C[∞]N[∞]) complexes through rollover metalation of the 2,2':6',3''- and 2,2':6',4''-terpy derivatives failed with both Pt(II) and Pd(II).

Reactions of [Pt(2,2':4',2''-terpy)Cl] (**Pt-1-Cl**) and [Pt(2,3':5',2''-terpy)Cl] (**Pt-2-Cl**) with phenylacetylene, CuI, and dry Et₃N in degassed CH₂Cl₂ under argon (Sonogashira conditions) provided the alkynyl complexes [Pt(2,2':4',2''-terpy)(C≡CPh)] (**Pt-1-CC**) and [Pt(2,3':5',2''-terpy)(C≡CPh)] (**Pt-2-CC**) at 14 and 87% yield, respectively.

These alkynyl complexes, together with the two Ni complexes, were the only products for which ¹H NMR characterisation was possible, while ¹³C NMR measurements were hampered by limited solubility in all organic solvents. For all other complexes, as outlined above, the poor, very poor, or completely lacking solubility of solvents such as non-polar benzene or toluene, fairly polar CH₂Cl₂ or tetrahydrofuran (THF), highly polar dimethylformamide (DMF) or dimethyl sulfoxide (DMSO), or even the protic MeOH or EtOH massively impeded characterisation and thus also potential applications in catalysis.

2.2. Crystal Structures

Single crystals of [Ni(2,3':5',2''-terpy)Br_{0.14}/OAc_{0.86}]·H₂O were obtained from the reaction mixture of the synthesis of [Ni(2,3':5',2''-terpy)Br] (**Ni-1-Br**). The acetate stems from the reaction medium (KOAc/K₂CO₃) and occupies the position of the ancillary ligand (coligand) together with B in a split position (Figure 1, data in Tables 2, S1 and S2; further views on the crystal structure are presented in Figures S2–S4 in the Supplementary Materials).

While this makes the Ni–Br/Ni–O distances meaningless, the other bonding parameters around Ni are very similar to the previously reported [Ni(dpbb)Br] and [Ni(dpbb)(OAc)] [50] (Table 2). The Ni–C1 bond is slightly shorter for the terpy complex, in line with the slightly reduced size of the carbanionic C atom through the influence of the electron-demanding N atom in the central ring. The crystal structure shows the typical head-to-tail π stacking (Figure 1a) [40–43,50–52], observed also for [Ni(dpbb)Br] and [Ni(dpbb)(OAc)] [50].

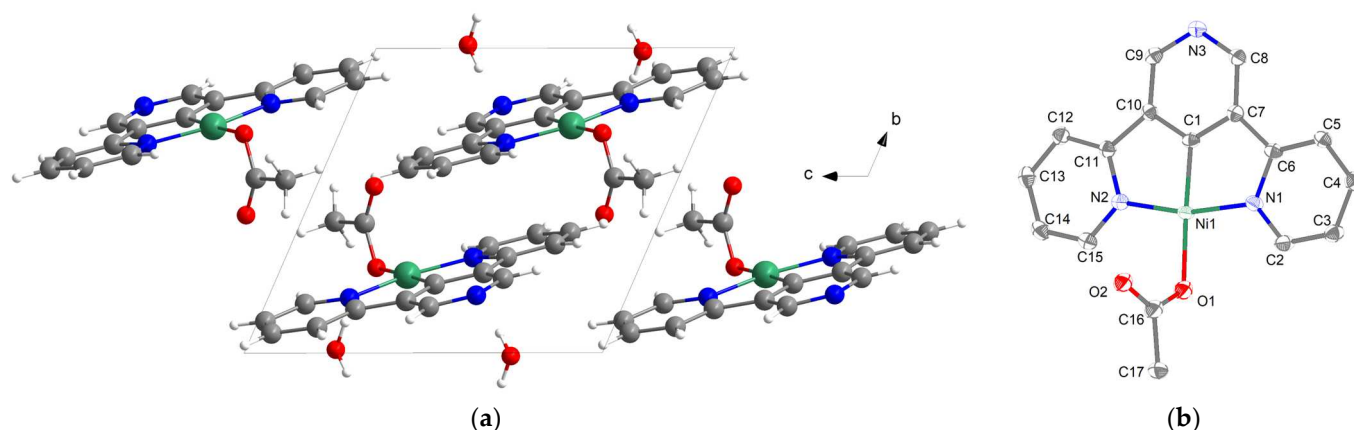


Figure 1. View of the crystal structure of [Ni(2,3':5',2''-terpy)Br_{0.14}/OAc_{0.86}]·H₂O along the *a*-axis (a) and ORTEP plot of the molecular structure with displacement ellipsoids at 50% probability; H atoms and the co-crystallised H₂O were omitted for clarity (b). In both views, only the OAc coligand is shown, which makes 86% of the OAc/Br disorder.

Table 2. Selected bond lengths (Å) and angles (°) ^a.

	[Ni(2,3':5',2''-terpy)Br _{0.13} /OAc _{0.87}]·H ₂ O	[Ni(dpbb)Br] ^b	[Ni(dpbb)(OAc)] ^b	[Pt(2,3':5',2''-terpyH)Cl]·Cl (Pt-H2-ClCl)	[Pt(terpy)Cl]·Cl·H ₂ O ^c	[Pt(dpbb)Cl] ^d
Distances/Å						
M1–C1	1.805(2)	1.8298(2)	1.8136(7)	1.896(8)	1.941(4) (N) ^e	1.907(8)
M1–N1	1.923(2)	1.9489(1)	1.9203(2)	2.039(8)	2.033(5)	2.033(6)
M1–N2	1.923(2)	1.9536(1)	1.9232(2)	2.025(8)	2.035(4)	2.041(6)
M1–O1	1.929(2)	-	1.9794(2)	-	-	-
M1–O2	2.962(3)	-	3.0331(2)	-	-	-
M1–X1	2.487(8)	2.3963(3)	-	2.382(2)	2.303(2)	2.417(2)
Angles/°						
C7–M1–N1	82.37(9)	81.94(7)	82.59(8)	81.2(4)	81.32(2) (N) ^e	80.1(3)
C7–M1–N2	82.24(9)	81.85(7)	82.48(8)	80.9(4)	80.97(2) (N) ^e	80.9(3)
N1–M1–O2	99.28(8)	-	98.31(7)	-	-	-
N2–M1–O2	96.05(8)	-	96.61(7)	-	-	-
N1–M1–X1	93.49(2)	97.83(4)	-	99.1(2)	98.63(2)	99.1(2)
N2–M1–X1	101.08(2)	98.39(4)	-	98.8(2)	99.09(2)	99.8(2)
N1–M1–N2	164.43(8)	163.78(6)	165.00(7)	162.1(3)	162.29(2)	161.1(2)
C7–M1–X1	160.03(2)	179.48(5)	-	179.6(3)	179.9(2) (N) ^e	179.0(2)
Sum ^o ^f	359.94(2)	360.01	359.99	360.00	360.01	359.90

^a From single crystal X-ray diffraction at 100 K, $\lambda = 0.71073$ Å. ^b From ref. [50]. ^c From ref. [68]. ^d From ref. [46]. ^e Not cyclometalated; therefore, N instead of C atoms. ^f Sum of angles around the central metal atom.

Single crystals of the compound [Pt(2,3':5',2''-terpyH)Cl]·Cl (Pt-H2-ClCl) were obtained by heating the yellow reaction product in a glass ampule containing acetic acid

under solvothermal conditions (Figure 2, data in Table 2, Tables S1 and S2; further views on the crystal structure are presented in Figures S10–S12 in the Supplementary Materials).

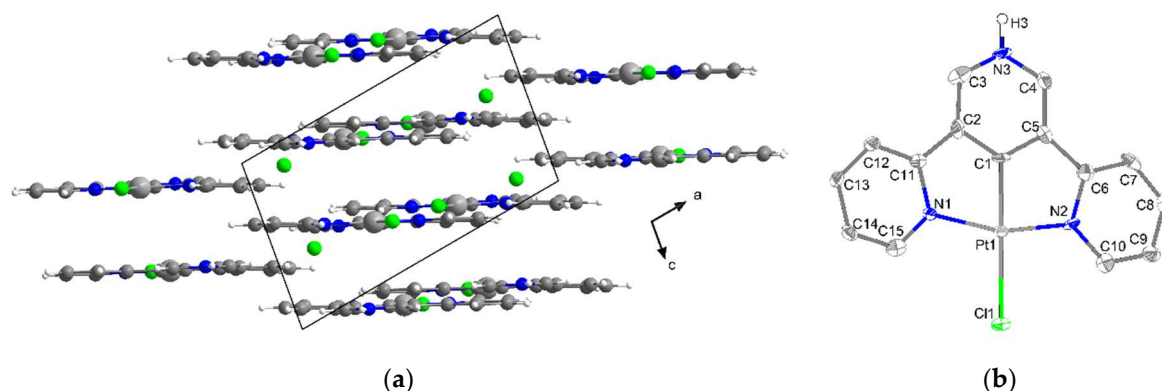


Figure 2. View of the crystal structure of $[\text{Pt}(2,3':5',2''\text{-terpyH})\text{Cl}]\cdot\text{Cl}$ (**Pt-H2-ClCl**) along the b -axis (a) and ORTEP plot of the molecular structure with displacement ellipsoids at 50% probability; H atoms other than the N–H and the Cl^- counterion were omitted for clarity (b).

The central pyridine-N function is protonated in the cationic complex $[\text{Pt}(2,3':5',2''\text{-terpyH})\text{Cl}]^+$ (**Pt-H2-ClCl**), which is due to the presence of the conc. HOAc. The highly polar solution together with the superior crystallisation properties of this salt-like compound over the neutral starting material $[\text{Pt}(2,3':5',2''\text{-terpy})\text{Cl}]$ (**Pt-2-Cl**) probably lead to the crystallisation of this unusual product. The central Pt–C bond of 1.896(8) Å in the cation $[\text{Pt}(2,3':5',2''\text{-terpyH})\text{Cl}]^+$ is shorter than the central Pt–N bond in the prototypical cation $[\text{Pt}(\text{terpy})\text{Cl}]^+$ (1.941(4) Å) [68], while the Pt–Cl bond is far longer (2.382(2) vs. 2.303(2) Å, Table 2). This is in line with the stronger *trans* influence of the central ring with its C1 carbanion bound to Pt. This is confirmed by the short Pt–C and the long Pt–Cl bond in $[\text{Pt}(\text{dpb})\text{Cl}]$ [46] (Table 1). In the crystal structure, $[\text{Pt}(2,3':5',2''\text{-terpyH})\text{Cl}]^+$ shows the same head-to-tail π stacking discussed above. For $[\text{Pt}(\text{dpb})\text{Cl}]$, such stacking was previously reported [46].

When trying to crystallise the material obtained for the targeted complex $[\text{Pd}(2,3':5',2''\text{-terpy})\text{Cl}]$ (**Pd-2-Cl**), we obtained the C^N bidentate cyclometalated complex $[\text{Pd}(2,3':5',2''\text{-terpy})\text{Cl}_2]$ (**Pd-H2-Cl2**) (Figure 3, data in Tables S1 and S2; further views on the crystal structure are presented in Figures S6–S8 in the Supplementary Materials).

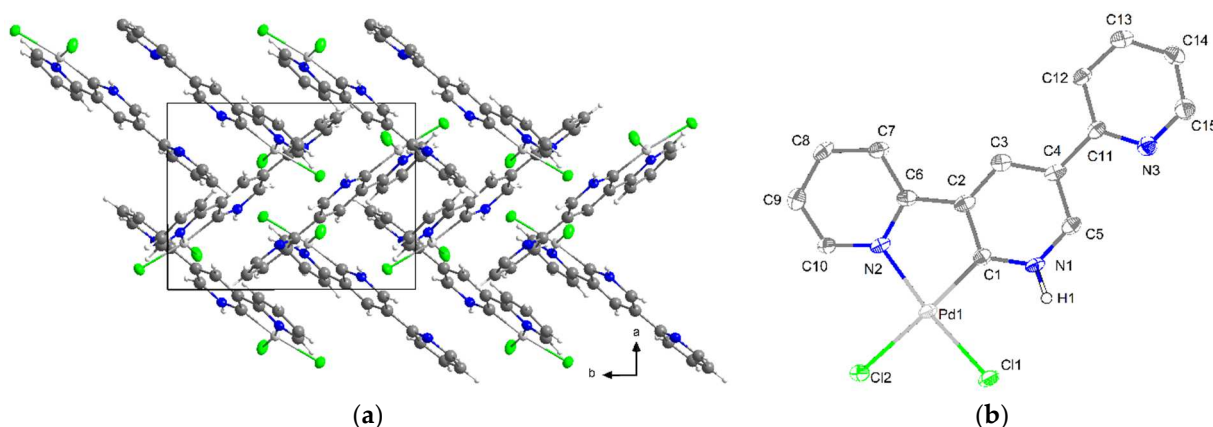


Figure 3. View of the crystal structure of $[\text{Pd}(2,3':5',2''\text{-terpyH})\text{Cl}_2]$ (**Pd-H2-Cl2**) along the c -axis (a) and ORTEP plot of the molecular structure with displacement ellipsoids at 50% probability; H atoms were omitted for clarity (b).

The cyclometalated $[\text{Pd}(\text{C}^{\wedge}\text{N})\text{Cl}_2]$ structural motif in $[\text{Pd}(2,3':5',2''\text{-terpyH})\text{Cl}_2]$ (**Pd-H2-Cl2**) is quite unique. A similar motif was found in the $[\text{Pd}(\text{phpy})\text{Cl}_2]^-$ (Hphpy = 2-

phenyl-pyridine) anion structurally characterised along with the cation $[\text{Te}(\text{phpy})\text{Cl}]^+$ [69], as well as in the dimer $[\text{Pd}(\text{phpy})(\mu\text{-Cl})_2\text{Pd}(\text{phpy})]$ [70], while many examples of mononuclear neutral $[\text{Pd}(\text{phpy})\text{Cl}(\text{L})]$ complexes with neutral ligands such as NH_3 , pyridines, or phosphines have also been reported [70–72]. Despite the specific Pd–C–NH–C structural unit **Pd-H2-Cl₂**, the essential bond parameters in these Pd(phpy) complexes and in the $[\text{Pd}(\text{phpy})\text{Cl}_2]^-$ anion are very similar. The Pd–Cl bonds' *trans* to the stronger donor C atom are markedly longer than the Pd–Cl bonds' *trans* to N, with 2.285(1) vs. 2.377(1) Å for **Pd-H2-Cl₂** and 2.37(1) vs. 2.49(1) Å for $[\text{Pd}(\text{phpy})\text{Cl}_2]^-$ [69]. The same is reported for the dimer $[\text{Pd}(\text{phpy})(\mu\text{-Cl})_2\text{Pd}(\text{phpy})]$ [70].

2.3. Electrochemistry

At first glance, all complexes show two reduction waves in the range of -1.5 to -3.0 V vs. ferrocene/ferrocenium (Figure 4, full data in Table S3; further cyclic voltammograms are presented in Figures S13–S18 in the Supplementary Materials). For the Pd and Pt complexes, the first reduction potentials lie around -1.5 V (Figure 4B, red and green bars), while for the Ni derivatives, far lower (more negative) values < -2.0 V were found (Figure 4B, blue bars). In view of similar complexes, these processes can be assigned to ligand (π^*)-centred reductions [10,25,43,50,52,73]. Compared with the ligands, the first reduction in the complexes is massively shifted to higher potentials by about 1 V for the Pt and Pd complexes and by about 0.5 V for the Ni derivatives. At the same time, while the Ni(II) complexes' oxidation waves assignable to a M(II)/M(III) redox pair were found at around 0.3 V, the same processes for the Pd(II) and Pt(II) derivatives are shifted to far higher potentials and could not be detected in THF solution due to solvent discharge at around 1.5 V. Nevertheless, assuming the solvent discharge limit as the minimal oxidation potential (Figure 4B), the experimental electrochemical gaps between the highest occupied molecular orbital (HOMO) and the lowest unoccupied molecular orbital (LUMO) lie higher than 3 V for the Pd(II) and Pt(II) complexes, while they can be unequivocally determined as 2.37 and 2.62 eV for the Ni(II) complexes. The lowest reduction potential and the lowest gap was found for $[\text{Ni}(2,3':5',2''\text{-terpy})\text{Br}]$ (**Ni-2-Br**), which is the symmetrical variant of the two Ni(II) complexes.

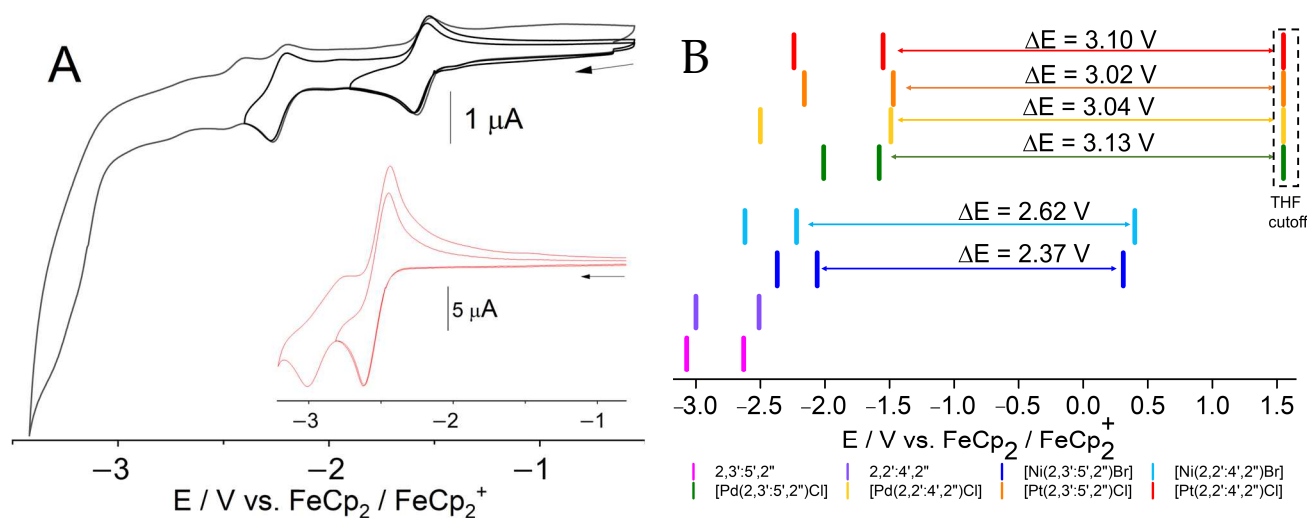


Figure 4. (A) Cyclic voltammograms of $[\text{Pt}(2,2':4',2''\text{-terpy})\text{Cl}]$ (**Pt-1-Cl**) (black trace) and 2,2':4',2''-terpy (red trace) in 0.1 M $n\text{-Bu}_4\text{NPF}_6/\text{THF}$ solution at 298 K and a scan rate of 100 mV/s. (B) Summarised selected redox potentials (full data in Table S3).

The first reduction potentials for the Pd(II) and Pt(II) complexes of the N[∞]C[∞]N-coordinated 2,3':5',2''- and 2,2':4',2''-terpy ligands are massively anodically shifted compared with the $[\text{Pt}(\text{dpb})\text{Cl}]$ (-2.17 V) [43,73] and the $[\text{Pd}(\text{Me}_2\text{dpb})\text{Cl}]$ (-2.34 V) [43] complexes (Table S3). This is fully in line with the central ligand core being a pyridine for the terpy derivatives;

thus, regardless of the metalation, the electron-accepting moiety is still a terpyridine, in contrast to the two pyridines separated by a phenyl unit in the dpb ligand [43,50]. For the Ni(II) derivatives, this is less pronounced, with [Ni(dpb)Cl] showing a reduction wave at -2.30 V [50].

The electrochemical gaps of the dpb Ni(II) and Pd(II) complexes lie in the same range as those found for the 2,3':5',2''- and 2,2':4',2''-terpy derivatives. It seems that the central pyridine in these ligands facilitates both ligand-centred reduction (superior π -accepting properties) and metal-centred oxidation (poorer σ -donating abilities) compared with the central phenyl in the dpb complexes to approximately the same extent. In contrast to this, for the Pt(II) complex [Pt(dpb)Cl], this gap lies at 2.58 eV [43], much smaller than that found for the terpy derivatives. This is due to the massively lowered oxidation potential of the dpb complex, which is decreased by about 0.5 V compared with the terpy complexes. This can be explained by the markedly higher stabilisation of the Pt 5d orbital compared with the Pd 4d and Ni 3d orbitals through the weaker σ donor capacity of the central pyridine unit in the terpy complexes, which is in line with the structural results discussed above.

2.4. UV-Vis Absorption Spectroscopy

The UV-vis absorption spectra of the Ni(II) complexes show several intense bands in the UV range up to 300 nm (Figure 5A). Since they also occur for the ligands (Table S4, Figure S19 in the Supplementary Material), we can assign them to transitions into π - π^* states. It is interesting to note that while the spectra of the ligands (including all derivatives in Scheme 3K,L) are pretty similar (Figure S19 in the Supplementary Material), the UV part for the complexes of the 2,3':5',2'' and 2,2':4',2'' ligands are markedly different (Figures 5 and S20–S22). We explain this through the different impact of planarisation through coordination, especially coinciding with the higher symmetry for the 2,3':5',2'' complexes. The UV bands are followed by broad, partially structured absorptions in the range of 300 to 500 nm, which can be assigned to transitions into metal-to-ligand charge transfer (MLCT) states, similar to what has been found for the N[^]C[^]N cyclometalated complexes [Ni(dpb)X] (X = Cl or Br) [50] and their derivatives [43]. Very similar long-wavelength MLCT bands are also found for the Pd and Pt complexes (Figure 5B, Table 3). The energies of the long-wavelength absorption bands decrease along the series Ni > Pt > Pd, as has also been observed for the [M(Me₂dpb)Cl] (M = Pt, Pd, Ni) complexes [43] and other series of complexes of the nickel group [44,64,65,74].

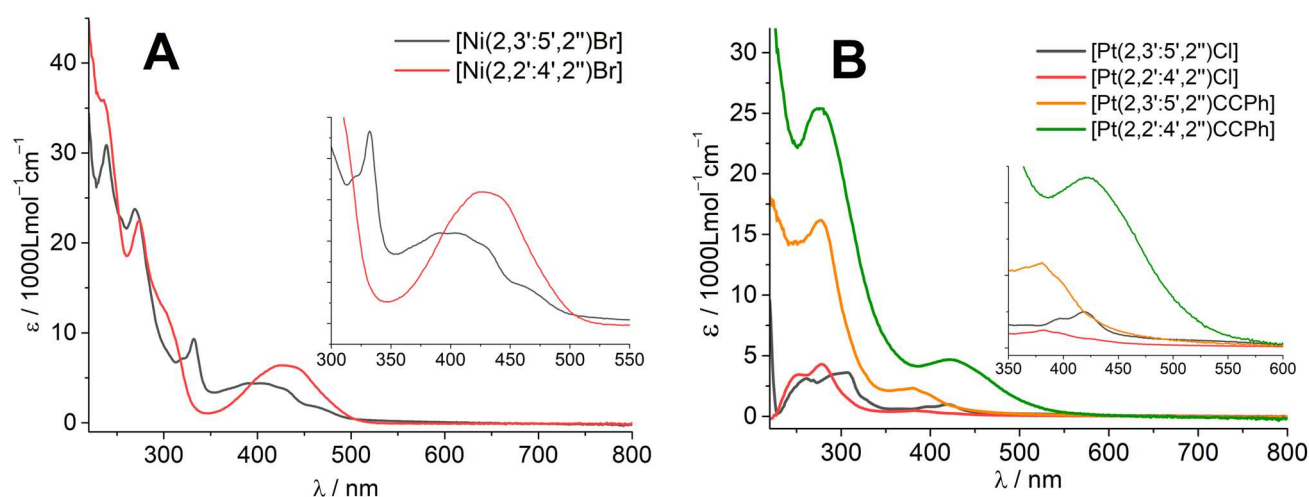


Figure 5. (A) UV-vis absorption spectra, wavelength (λ) against molar extinction coefficient (ϵ), of [Ni(Y-terpy)Br] (Y = 2,3':5',2'' (Ni-1-Br) and 2,2':4',2'' (Ni-2-Br)) and (B) [Pt(Y-terpy)(X)] (Y = 2,3':5',2'' and 2,2':4',2''; X = Cl (Pt-1- or -2-Cl) or C \equiv CPh (Pt-1- or -2-CC)) in THF solution.

Table 3. Long-wavelength UV-vis absorption maxima and the optical and electrochemical gaps of complexes [M(Y-terpy)X] and related complexes ^a.

[M(Y-terpy)X]	λ (nm)	ΔE_{opt} (eV)	ΔE_{redox} (eV)	$\Delta\Delta$
M = Ni, X = Br				
Y = 2,3':5',2'' (Ni-1-Br)	466 (1.7)	2.48	2.37	0.11
Y = 2,2':4',2'' (Ni-2-Br)	431 (6.4)	2.87	2.62	0.25
[Ni(dpb)Br] ^b	433 (5.6)	2.86	2.37	0.49
M = Pd, X = Cl				
Y = 2,3':5',2'' (Pd-1-Cl)	389 (2.6)	3.19	3.13	0.06
Y = 2,2':4',2'' (Pd-2-Cl)	355 (6.6)	3.49	3.04	0.45
[Pd(Me ₂ dpb)Cl] ^c	375 (1.2)	3.31	3.08	0.23
M = Pt, X = Cl				
Y = 2,3':5',2'' (Pt-1-Cl)	396 (0.8)	3.13	3.02	0.11
Y = 2,2':4',2'' (Pt-2-Cl)	427 (0.4)	2.90	3.10	0.20
[Pt(dpb)Cl] ^d	402 (7.0)	3.08	2.49	0.59
M = Pt, X = C≡CPh				
Y = 2,3':5',2'' (Pt-1-CC)	395 (1.9)	3.14		
Y = 2,2':4',2'' (Pt-2-CC)	424 (4.6)	2.92		
[Pt(dpb)(C≡CPh)] ^e	391 (9.3)	3.17		

^a Absorption maxima λ in nm in THF solution at rt; molar absorption coefficient ϵ in 1000 L mol⁻¹ cm⁻¹. ^b From ref. [50]. ^c From ref. [43]. ^d From refs. [73,75]. ^e From ref. [76], measured in CH₂Cl₂. Optical band gap ΔE_{opt} was obtained from the long-wavelength absorptions.

When replacing the Cl ligands in the Pt complexes with phenyl-ethynyl, a general increase in intensities was recorded (Figure 5B). For the symmetric 2,3':5',2'' complexes (Pt-2-Cl to Pt-2-CC), we found a blue shift for the long-wavelength absorptions from 420 to 380 nm, while for the 2,2':4',2'' derivatives, replacement of Cl with C≡CPh (Pt-2-Cl to Pt-2-CC) resulted in a red shift from 380 to 430 nm. We assign this remarkable difference to the different symmetry of the two pairs of complexes, as discussed already for the comparison between ligand spectra and the spectra of the Ni, Pd, and Pt complexes. The broad π - π^* absorptions of the Pt phenyl-ethynyl complexes Pt-1-CC and Pt-2-CC are very similar in energy.

For the long-wavelength maxima, we calculated the optical gaps (ΔE_{opt}) (Table 3). They range from 2.48 to 3.49 eV along the series of metals Ni < Pt < Pd and they are markedly smaller than the electrochemical gaps (ΔE_{redox}), which is in line with the Franck-Condon excitation leading into higher vibronic states, while the redox gap represents relaxed molecule geometries for both reduced and oxidised states. The difference represents reorganisation energy and is generally smaller for the 2,3':5',2''-terpy complexes than for the 2,2':4',2'' derivatives and the dpb complexes.

3. Materials and Methods

3.1. Instrumentation

¹H, ¹³C, and correlation spectra were recorded either on a Bruker Avance II 300 MHz (¹H: 300 MHz, ¹³C: 75 MHz) equipped with a double resonance (BBFO) 5 mm observe probe head with a z-gradient coil or on a Bruker Avance III 499 (¹H: 499 MHz, ¹³C: 125 MHz) using a TCI Prodigy 5 mm probe head with a z-gradient coil (Bruker, Rheinhausen, Germany). Chemical shifts were relative to TMS (¹H, ¹³C). UV-vis absorption spectra were recorded on a Varian Cary 05E spectrophotometer (Varian Medical Systems, Darmstadt, Germany). Elemental analyses were conducted using an HEKAtech CHNS EuroEA 3000 analyser (HEKAtech, Wegberg, Germany). EI-MS spectra in the positive mode were measured

using a Finnigan MAT 95 mass spectrometer at 70 eV (Thermo Finnigan Mat, Bremen, Germany). HR-ESI-MS spectra in the positive mode were measured using a Thermo Scientific LTW Orbitrap XL mass spectrometer at 70 eV (ThermoFisher Scientific, Waltham, MA, USA). Simulations were performed using ISOPRO 3.0 (Mike Senko, Sunnyvale, CA, USA). Electrochemical measurements were carried out in 0.1 M *n*-Bu₄NPF₆ solution in THF (tetrahydrofuran) using a three-electrode configuration (glassy carbon electrode, Pt counter electrode, Ag/AgCl reference) and a Metrohm Autolab PGSTAT30 or μ Stat400 potentiostat (Metrohm, Filderstadt, Germany). The potentials were referenced against the ferrocene/ferrocenium redox couple as an internal standard.

3.2. Single Crystal Structure Analysis by X-ray Diffractometry (XRD)

Crystals of [Ni(2,3',5':2''-terpy)Br_{0.14}/OAc_{0.86}]·H₂O were obtained by isothermal evaporation of the complex dissolved in CH₂Cl₂. [Pd(2,3':5',2''-terpyH)Cl₂] and [Pt(2,3':5',2''-terpyH)Cl]·Cl were obtained by heating the complexes in acetic acid in glass ampoules, ramping to 200 °C over 12 h, and then cooling to room temperature over the course of 48 h. X-ray diffraction experiments were performed at 100(2) K, employing a Bruker D8 Venture including a Bruker Photon 100 CMOS detector using Mo-K α radiation ($\lambda = 0.71073$ Å) (Bruker, Rheinhausen, Germany). The crystal data were collected using APEX3 v2015.5-2 [77]. The structures were solved by dual space methods using SHELXT (Sheldrick 2015) [78] and the refinement was carried out with SHELXL 2017, employing the full-matrix least-squares methods on $F_0^2 \geq 2\sigma(F_0^2)$ [79]. The non-hydrogen atoms were refined with anisotropic displacement parameters without any constraints. The hydrogen atoms were included through the use of appropriate riding models. The presence of the N–H proton in the [Pt(2,3':5',2''-terpyH)Cl]·Cl complex was attributed to the observed residual electron density and the necessity of balancing the charge of the chloride anion found in the crystal structure. The same is true for the N–H proton in the complex [Pd(2,3':5',2''-terpyH)Cl₂]. Data concerning the structure solutions and refinements can be obtained for [Ni(2,3':5',2''-terpy)Br_{0.14}/OAc_{0.86}]·H₂O (CCDC 2250815), [Pd(2,3':5',2''-terpyH)Cl₂] (CCDC 2250813), and [Pt(2,3':5',2''-terpyH)Cl]·Cl (CCDC 2250812) free of charge at <https://summary.ccdc.cam.ac.uk/structure-summary-form> or from the Cambridge Crystallographic Data Centre, Cambridge, UK (e-mail: deposit@ccdc.cam.ac.uk).

3.3. Materials

All chemicals were used as purchased without any further purification. Reactions sensitive to oxygen or water were carried out under argon gas atmosphere (99.998%, Linde, Pullach, Germany) using the *Schlenk* technique. Dry THF was distilled over Na/K (alloy 3:7) before use. Dry *p*-xylene was freshly distilled over sodium. Other dry solvents were dried using the solvent purification system MRBAUN MB SPS-800 (MBraun, Garching, Germany).

3.4. Syntheses

3.4.1. Syntheses of Ligand Precursors and Terpy Ligands

The synthesis of ligand precursors and terpy ligands is described in the Supplementary Materials.

3.4.2. Synthesis of the Ni(II) Complexes [Ni(2,3':5',2''-terpy)Br] and [Ni(2,2':4',2''-terpy)Br]—General Description

In an inert flask equipped with a water trap filled with a molecular sieve (3 Å), anhydrous NiBr₂ (1.3 eq.), KOAc (1.0 eq.), K₂CO₃ (1.0 eq.), and the terpy ligand (1.0 eq.) were added. Distilled dry *p*-xylene (200 mL) was added and the mixture heated to reflux for 72 h. After cooling to room temperature, the precipitated solid was filtered off and washed once with *p*-xylene, and the product was extracted using THF before being washed with CH₂Cl₂ over a syringe filter (PTFE, 0.45 μ m pore size). The solvent was evaporated and the product isolated as a microcrystalline powder.

[Ni(2,2':4',2''-terpyridine)Br] (Ni-1-Br): Obtained from 110 mg (0.50 mmol) NiBr₂, 49.1 mg (0.50 mmol) KOAc, 69.0 mg (0.50 mmol) K₂CO₃, and 117 mg (0.50 mmol) 2,2':4',2''-terpyridine. Yield: 102 mg (0.28 mmol, 55%), red powder. Elemental analysis found (calcd. for C₁₅H₁₀N₃NiBr, M = 370.86 g mol⁻¹) C, 48.52 (48.58); H, 2.70 (2.72); N, 11.31 (11.33). ¹H NMR (CDCl₃, 300 Mhz): δ/ppm = 9.37 (d, ³J = 5.7 Hz, 1H, H1); 9.28 (d, ³J = 5.6 Hz, 1H, H15); 8.35 (d, ³J = 5.0 Hz, 1H, H7); 7.95–7.88 (m, 3H, H3, H8, H13); 7.70 (d, ³J = 7.8 Hz, 1H, H4); 7.26 (q, ³J = 7.8 Hz, 2H, H2, H14); 7.19 (d, ³J = 5.0 Hz, 1H, H12). HR-ESI-MS (70 eV): *m/z* = 403; 21 [M+MeOH+H]⁺; 393.22 [M+Na]⁺; 290.02 [M–Br]⁺.

[Ni(2,3':5',2''-terpyridine)Br] (Ni-2-Br): Obtained from 110 mg (0.50 mmol) NiBr₂, 49.1 mg (0.50 mmol) KOAc, 69.0 mg (0.50 mmol) K₂CO₃, and 117 mg (0.50 mmol) 2,2':4',2''-terpyridine. Yield: 111 mg (0.30 mmol, 60%), orange powder. Elemental analysis found (calcd. for C₁₅H₁₀N₃NiBr, M = 370.86 g mol⁻¹) C, 48.55 (48.58); H, 2.73 (2.72); N, 11.35 (11.33). ¹H NMR (CDCl₃, 300 Mhz): δ/ppm = 8.44 (s, 2H, H1, H1'); 8.15 (s, 2H, H7, H7'); 8.00 (t, ³J = 7.7 Hz, 2H, H3, H3'); 7.88 (d, ³J = 7.8 Hz, 2H, H4, H4'); 7.24 (t, ³J = 6.6 Hz, 2H, H2, H2'). EI-MS (70 eV): *m/z* = 370.94 [M+H]⁺; 324.99 [M–Br+MeOH]⁺; 290.02 [M–Br]⁺; 234.09 [Ligand+H]⁺.

3.4.3. Synthesis of the Pd(II) Complexes [Pd(2,3':5',2''-terpy)Cl] and [Pd(2,2':4',2''-terpy)Cl]—General Description

The ligands (1.00 eq.) and K₂PdCl₄ (1.00 eq.) were added to glacial acetic acid and heated to reflux overnight under exclusion of light. After cooling to room temperature, the formed precipitates were filtered off over a silica filter pad and washed with acetic acid, MeOH, and diethyl ether. The products were obtained as red or yellow powders.

[Pd(2,2':4',2''-terpyridine)Cl] (Pd-1-Cl): Obtained from 97.9 mg (0.30 mmol) K₂PdCl₄ and 69.9 mg (0.30 mmol) 2,2':4',2''-terpyridine in 10 mL of glacial acetic acid, reflux for 21 h. Yield: 94.3 mg (0.25 mmol, 84%), red powder. Elemental analysis found (calcd. for C₁₅H₁₀N₃PdCl, M = 374.14 g mol⁻¹) C, 48.17 (48.15); H, 2.61 (2.69); N, 11.21 (11.23). HR-ESI-MS (70 eV): *m/z* = 453.98 [M+DMSO+H]⁺; 407.99 [M+MeOH+H]⁺; 393.98 [M+Na]⁺; 372.97 [M+H]⁺; 338.99 [M–Cl]⁺.

[Pd(2,3':5',2''-terpyridine)Cl] (Pd-2-Cl): Obtained from 97.9 mg (0.30 mmol) of K₂PdCl₄ and 69.9 mg (0.30 mmol) of 2,3':4',2''-terpyridine in 10 mL of glacial acetic acid heated under reflux for 17 h under exclusion of light. Yield: 62.3 mg (0.17 mmol, 57%), yellow powder. Elemental analysis found (calcd. for C₁₅H₁₀N₃PdCl, M = 374.14 g mol⁻¹) C, 48.24 (48.15); H, 2.64 (2.69); N, 11.17 (11.23). HR-ESI-MS (70 eV): *m/z* = 372.97 [M+H]⁺; 234.10 [ligand+H]⁺. EI-MS: (70 eV) 233.09 [ligand]⁺.

3.4.4. Synthesis of the Pt(II) Complexes [Pt(2,3':5',2''-terpy)Cl] and [Pt(2,2':4',2''-terpy)Cl]—General Description

The ligand (1.20 eq.) and K₂PtCl₄ (1.00 eq.) were added to glacial acetic acid and heated under reflux for 3 days. After cooling to room temperature, the formed precipitate was filtered off over a silica filter pad and washed with acetic acid, MeOH, and Et₂O. The product was obtained as a yellow or red powder.

[Pt(2,2':4',2''-terpyridine)Cl] (Pt-1-Cl): Obtained from 208 mg (0.50 mmol, 1.00 eq.) K₂PtCl₄ and 140 mg (0.60 mmol, 1.20 eq.) 2,2':4',2''-terpyridine in 10 mL of glacial acetic acid heated under reflux for 114 h. Yield: 111 mg (0.24 mmol, 40%), red powder. Elemental analysis found (calcd. for C₁₅H₁₀N₃PtCl, M = 462.80 g mol⁻¹) C, 38.99 (38.93); H, 2.15 (2.18); N, 9.09 (9.08). HR-ESI-MS (70 eV): *m/z* = 541.04 [M+DMSO+H]⁺; 494.03 [M+MeOH+H]⁺; 463.02 [M+H]⁺; 427.04 [M–Cl]⁺.

[Pt(2,3':5',2''-terpyridine)Cl] (Pt-2-Cl): Obtained from 33.6 mg (144 μmol, 1.20 eq.) 2,3':5',2''-terpyridine and 49.8 mg (0.12 mmol, 1.00 eq.) K₂PtCl₄ added to 10 mL of glacial acetic acid. The mixture was heated to reflux for 64 h. Yield: 35.0 mg (76.0 μmol, 63%), yellow powder. Elemental analysis found (calculated for C₁₅H₁₀N₃PtCl, M = 462.80 g mol⁻¹) C, 39.14 (38.93); H, 2.33 (2.18); N, 8.92 (9.08). HR-ESI-MS (70 eV): *m/z* = 463.02 [M+H]⁺.

3.4.5. Synthesis of the Pt(II) Complexes [Pt(2,3':5',2''-terpy)(C≡CPh)] and [Pt(2,2':4',2''-terpy)(C≡CPh)]—General Description

The chloride complex (1.00 eq.) was added to phenylacetylene (3.00 eq.), CuI (8 mol%), and dry Et₃N (65.0 eq.) in degassed CH₂Cl₂ under argon. The mixture was stirred at room temperature under exclusion of light for 18 h. Et₂O was added and the formed precipitate was filtered off and washed with Et₂O and *n*-pentane. The residue was redissolved in CH₂Cl₂ and washed with distilled water. The organic phase was separated and the solvent evaporated off to yield the product as an orange powder.

[Pt(2,2':4',2''-terpyridine)(C≡CPh)] (Pt-1-CC): Obtained from 50.0 mg (0.11 mmol, 1.00 eq.) of the chlorido complex, 36.0 μL (0.33 mmol, 3.00 eq.) phenylacetylene, 1.67 mg (8.80 μmol, 8 mol%) CuI, and 1.00 mL (7.20 mmol, 65.0 eq.) dry Et₃N in 20.0 mL degassed and dried CH₂Cl₂. Yield: 7.90 mg (15.0 μmol, 14%), orange powder. Elemental analysis found (calcd. for C₂₃H₁₅N₃Pt, M = 528.48 g mol⁻¹) C, 51.97 (52.27); H, 2.82 (2.82); N, 7.99 (7.95). ¹H NMR (CDCl₃, 300 MHz): δ/ppm = 9.74 (dd, ³J = 10.7 Hz, ⁴J = 5.7 Hz, 2H); 8.91 (s, 1H); 8.79 (d, ³J = 3.5 Hz, 1H); 8.31 (d, ³J = 8.1 Hz, 1H); 8.19 (t, ³J = 7.8 Hz, 1H); 8.12 (d, ³J = 5.8 Hz, 1H); 8.04 (d, ³J = 7.9 Hz, 1H); 7.89 (t, ³J = 7.8 Hz, 1H); 7.62 (t, ³J = 6.1 Hz, 1H); 7.51–7.45 (m, 2H); 7.29 (q, ³J = 7.7 Hz, 1H); 7.21–7.15 (m, 2H). HR-ESI-MS (70 eV): *m/z* = 529.12 [M+H]⁺; 505.06 [M–coligand+DMSO+H]⁺; 234.1 [ligand+H]⁺.

[Pt(2,3':5',2''-terpyridine)(C≡CPh)] (Pt-2-CC): Obtained from 50.0 mg (0.11 mmol, 1.00 eq.) of the chloride complex, 36.0 μL (0.33 mmol, 3.00 eq.) phenylacetylene, 1.67 mg (8.80 μmol, 8 mol%) CuI, and 1.00 mL (7.20 mmol, 65.0 eq.) dry Et₃N in 20.0 mL degassed and dried CH₂Cl₂. Yield: 50.5 mg (96.0 μmol, 87%), orange powder. Elemental analysis found (calcd. for C₂₃H₁₅N₃Pt, M = 528.48 g mol⁻¹) C, 52.07 (52.27); H, 2.77 (2.82); N, 7.89 (7.95). ¹H NMR (CDCl₃, 300 MHz): δ/ppm = 9.91 (d, ³J = 2.0 Hz, 2H); 9.16 (s, 1H); 8.73 (d, ³J = 4.8 Hz, 2H); 7.94 (d, ³J = 7.9 Hz, 3H); 7.80 (t, ³J = 8.0 Hz, 2H); 7.37–7.28 (m, 3H); 7.19–7.10 (m, 2H). HR-ESI-MS (70 eV): *m/z* = 529.09 [M+H]⁺; 400.23 [M–coligand]⁺.

4. Conclusions

In this study, we attempted to cyclometalate stereoisomers of the well-known tridentate N[^]N[^]N ligand 2,2':6',2''-terpyridine (terpy), the two 2,2':6',3'' and 2,2':6',4'' isomers for potential rollover C[^]N[^]N cyclometalation and the 2,2':4',2'' and 2,3':5',2'' isomers for potential N[^]C[^]N cyclometalation, using Ni(II), Pd(II), and Pt(II).

Applying established procedures, we obtained [M(N[^]C[^]N)X] complexes for the 2,3':5',2'' and 2,2':4',2'' isomers with M = Ni, X = Br; Pd, X = Cl, and Pt, X = Cl or C≡CPh. Attempts to produce the [M(C[^]N[^]N)X] complexes with the 2,2':6',3''- and 2,2':6',4''-terpy derivatives failed. This is remarkable as the related 6-phenyl-2,2'-bipyridine (HPhbpy) ligand was successfully cyclometalated in previous studies and the N[^]N pre-coordination that has been found beneficial for the cyclometalation of HPhbpy should also be available for the 2,2':6',3''- and 2,2':6',4''-terpy isomers. As deprotonation of a pyridine moiety in the terpy derivatives should be easier compared with the phenyl group of HPhbpy, we can rule out electronic effects. Instead, we suspect that the required rollover mechanism, which is the rotation of the pending pyridine unit to approach the C–H function to be activated into the proximity of the metal, is hampered. For the successfully N[^]C[^]N cyclometalated 2,2':4',2''- and 2,3':5',2''-terpy derivatives, such rollover metalation is not necessary. We will study the possible mechanism for the cyclometalation of terpy derivatives in the near future using density functional theory (DFT) calculations, with particular focus on comparing rollover to non-rollover variants energetically.

When comparing the electronic properties of the [M(N[^]C[^]N)X] complexes of the 2,3':5',2'' and 2,2':4',2'' isomers as represented by their electrochemical potentials and their long-wavelength absorptions, we found that the central pyridine moiety has superior π-accepting and poorer σ-donating properties compared with the central phenyl unit of the prototypical N[^]C[^]N cyclometalating dpb⁻ ligand (Hdpb = 2,6-dipyridylbenzene), as expected. For the Pd and Ni complexes, both effects have a similar magnitude, which results in almost identical electrochemical gaps for the terpy complexes and the dpb

derivatives and therefore very similar overall electrochemical stability. The markedly less negative reduction potentials of these cyclometalated terpy Ni complexes might be beneficial for Negishi-type C–C cross-coupling catalysis. The same might be true for the Pd derivatives in Kumada-type coupling catalysis. However, the solubility of all the herein reported complexes was very poor. This poor solubility partially or fully hampered proper characterisation, and in some cases it is not even clear if the targeted products were obtained at all. Thus, for future studies on the cyclometalation of terpy derivatives and their potential applications, substituted terpy derivatives must be used to render the target complexes soluble in the desired media.

Supplementary Materials: The following supporting information can be downloaded at: <https://www.mdpi.com/article/10.3390/inorganics11040174/s1>, Details on the syntheses. Supplementary Figures—Figure S1: Molecular structure of [Ni(2,3':5',2''-terpy)Br_{0.14}/OAc_{0.86}].H₂O; Figure S2: View of the crystal structure of [Ni(2,3':5',2''-terpy)Br_{0.14}/OAc_{0.86}].H₂O along the crystallographic *a*-axis; Figure S3: View of the crystal structure of [Ni(2,3':5',2''-terpy)Br_{0.14}/acetate_{0.86}].H₂O along the crystallographic *b*-axis; Figure S4: View of the crystal structure of [Ni(2,3':5',2''-terpy)Br_{0.14}/acetate_{0.86}].H₂O along the crystallographic *c*-axis; Figure S5: Molecular structure of [Pd(2,3':5',2''-terpyH)Cl₂]; Figure S6: View of the crystal structure of [Pd(2,3':5',2''-terpyH)Cl₂] along the crystallographic *a*-axis; Figure S7: View of the crystal structure of [Pd(2,3':5',2''-terpyH)Cl₂] along the crystallographic *b*-axis; Figure S8: View of the crystal structure of [Pd(2,3':5',2''-terpyH)Cl₂] along the crystallographic *c*-axis; Figure S9: Molecular structure of [Pt(2,3':5',2''-terpyH)Cl]Cl; Figure S10: View of the crystal structure of [Pt(2,3':5',2''-terpyH)Cl]Cl along the crystallographic *a*-axis; Figure S11: View of the crystal structure of [Pt(2,3':5',2''-terpyH)Cl]Cl along the crystallographic *b*-axis; Figure S12: View of the crystal structure of [Pt(2,3':5',2''-terpyH)Cl]Cl along the crystallographic *c*-axis; Figure S13: Cyclic voltammograms of 2,2':6',3''-terpy and 2,2':6',4''-terpy; Figure S14: Cyclic voltammograms of 2,3':5',2''-terpy and 2,2':4',2''-terpy; Figure S15: Cyclic voltammograms of [Ni(2,3':5',2''-terpy)Br] and [Ni(2,2':4',2''-terpy)Br]; Figure S16: Cyclic voltammograms of [Pd(2,3':5',2''-terpy)Cl] and [Pd(2,2':4',2''-terpy)Cl]; Figure S17: Cyclic voltammograms of [Pt(2,3':5',2''-terpy)Cl] and [Pt(2,2':4',2''-terpy)Cl]; Figure S18: Cyclic voltammograms of [Pt(2,2':4',2''-terpy)(C≡CPh)]; Figure S19: UV-vis absorption spectra of the terpyridine ligands in THF; Figure S20: UV-vis absorption spectra of the [Pd(Y-terpy)Cl] complexes in THF; Figure S21: UV-vis absorption spectra of the [Pt(Y-terpy)Cl] complexes in THF; Figure S22: UV-vis absorption spectra of the [Pt(Y-terpy)CCPh] complexes in THF. Supplementary Tables—Table S1: Crystal data and structure refinement for [M(Y-terpy)X] complexes; Table S2: Selected bond lengths (Å) and angles (°) for [M(Y-terpy)X] complexes; Table S3: Redox potentials of the [M(Y-terpy)X] (M = Pt, Pd, Ni) complexes and related complexes; Table S4: Selected UV-vis absorption maxima of Y-terpy ligands, [M(Y-terpy)X] complexes, and related complexes.

Author Contributions: Conceptualisation, A.K.; methodology, L.P., L.K., M.W. and A.K.; investigation, L.P. and T.L.; resources, M.W. and A.K.; data curation, L.P., L.K., T.L. and A.K.; visualisation, L.P. and A.K.; supervision and project administration, M.W. and A.K.; writing—original draft, L.P. and A.K.; writing—review and editing, A.K. All authors have read and agreed to the published version of the manuscript.

Funding: This research was funded by the Deutsche Forschungsgemeinschaft (DFG Priority Programme 2102 “Light-controlled Reactivity of Metal Complexes”), KL1194/16-1 and 16-2 (AK).

Data Availability Statement: Data may be requested directly from the authors.

Acknowledgments: At the Department of Chemistry, University of Cologne, we thank Silke Kremer (XRD facility) for measuring XRD datasets, and Sean S. Sebastian for assistance in the refinement of the XRD data.

Conflicts of Interest: The authors declare no competing financial interest.

References

1. Rogge, T.; Kaplaneris, N.; Chatani, N.; Kim, J.; Chang, S.; Punji, B.; Schafer, L.L.; Musaev, D.G.; Wencel-Delord, J.; Roberts, C.A.; et al. C–H activation. *Nat. Rev. Methods Primers* **2021**, *1*, 43. [CrossRef]
2. Corio, A.; Gravier-Pelletier, C.; Busca, P. Regioselective Functionalization of Quinolines through C-H Activation: A Comprehensive Review. *Molecules* **2021**, *26*, 5467. [CrossRef] [PubMed]

3. Rej, S.; Das, A.; Chatani, N. Strategic evolution in transition metal-catalyzed directed C–H bond activation and future directions. *Coord. Chem. Rev.* **2021**, *431*, 213683. [[CrossRef](#)]
4. Zucca, A.; Pilo, M.I. Rollover Cyclometalation as a Valuable Tool for Regioselective C–H Bond Activation and Functionalization. *Molecules* **2021**, *26*, 328. [[CrossRef](#)] [[PubMed](#)]
5. Baudoin, O. Multiple Catalytic C–H Bond Functionalization for Natural Product Synthesis. *Angew. Chem. Int. Ed.* **2020**, *59*, 17798–17809. [[CrossRef](#)]
6. Sambiagio, C.; Schönbauer, D.; Blicek, R.; Dao-Huy, T.; Pototschnig, G.; Schaaf, P.; Wiesinger, T.; Zia, M.F.; Wencel-Delord, J.; Besset, T.; et al. A comprehensive overview of directing groups applied in metal-catalysed C–H functionalisation chemistry. *Chem. Soc. Rev.* **2018**, *47*, 6603–6743. [[CrossRef](#)]
7. Zakis, J.M.; Smejkal, T.; Wencel-Delord, J. Cyclometallated complexes as catalysts for C–H activation and functionalization. *Chem. Commun.* **2022**, *58*, 483–490. [[CrossRef](#)]
8. Winter, A.; Schubert, U.S. Metal-Terpyridine Complexes in Catalytic Application—A Spotlight on the Last Decade. *ChemCatChem* **2020**, *12*, 2890–2941. [[CrossRef](#)]
9. Wei, C.; He, Y.; Shi, X.; Song, Z. Terpyridine-metal complexes: Applications in catalysis and supramolecular chemistry. *Coord. Chem. Rev.* **2019**, *385*, 1–19. [[CrossRef](#)]
10. Budnikova, Y.H.; Vicić, D.A.; Klein, A. Exploring mechanisms in Ni terpyridine catalysed C–C cross coupling reactions—a review. *Inorganics* **2018**, *6*, 18. [[CrossRef](#)]
11. Leist, M.; Kerner, C.; Taghizadeh Ghoochany, L.; Farsadpour, S.; Fizia, A.; Neu, J.P.; Schön, F.; Sun, Y.; Oelkers, B.; Lang, J.; et al. Roll-over cyclometalation: A versatile tool to enhance the catalytic activity of transition metal complexes. *J. Organomet. Chem.* **2018**, *863*, 30–43. [[CrossRef](#)]
12. Winter, A.; Hager, M.D.; Newkome, G.R.; Schubert, U.S. The Marriage of Terpyridines and Inorganic Nanoparticles: Synthetic Aspects, Characterization Techniques, and Potential Applications. *Adv. Mater.* **2011**, *23*, 5728–5748. [[CrossRef](#)]
13. Housecroft, C.E.; Constable, E.C. The terpyridine isomer game: From chelate to coordination network building block. *Chem. Commun.* **2020**, *56*, 10786–10794. [[CrossRef](#)]
14. Rocco, D.; Prescimone, A.; Constable, E.C.; Housecroft, C.E. Adapting (4,4) Networks through Substituent Effects and Conformationally Flexible 3,2':6',3''-Terpyridines. *Molecules* **2021**, *26*, 6337. [[CrossRef](#)]
15. Agosti, A.; Kuna, E.; Bergamini, G. Divergent Terpyridine-Based Coordination for the Construction of Photoactive Supramolecular Structures. *Eur. J. Inorg. Chem.* **2019**, 577–584. [[CrossRef](#)]
16. Gao, Z.; Han, Y.; Gao, Z.; Wang, F. Multicomponent Assembled Systems Based on Platinum(II) Terpyridine Complexes. *Acc. Chem. Res.* **2018**, *51*, 2719–2729. [[CrossRef](#)]
17. Chen, Z.; Chan, M.H.-Y.; Yam, V.W.-W. Stimuli-Responsive Two-Dimensional Supramolecular Polymers Based on Trinuclear Platinum(II) Scaffolds: Reversible Modulation of Photoluminescence, Cavity Size, and Water Permeability. *J. Am. Chem. Soc.* **2020**, *142*, 16471–16478. [[CrossRef](#)]
18. Yam, V.W.-W.; Chan, A.K.-W.; Hong, E.Y.-H. Charge-transfer processes in metal complexes enable luminescence and memory functions. *Nat. Rev. Chem.* **2020**, *4*, 528–541. [[CrossRef](#)]
19. Yam, V.W.-W.; Au, V.K.-M.; Leung, S.Y.-L. Light-Emitting Self-Assembled Materials Based on d⁸ and d¹⁰ Transition Metal Complexes. *Chem. Rev.* **2015**, *115*, 7589–7728. [[CrossRef](#)]
20. Barker, N.M.; Taylor, S.D.; Ferguson, E.; Krause, J.A.; Oliver, A.G.; Connick, W.B.; Zhang, P. Water's Role in Polymorphic Platinum(II) Complexes. *Inorg. Chem.* **2021**, *60*, 14731–14743. [[CrossRef](#)]
21. Yam, V.W.-W.; Law, A.S.-Y. Luminescent d⁸ metal complexes of platinum(II) and gold(III): From photophysics to photofunctional materials and probes. *Coord. Chem. Rev.* **2020**, *414*, 213298. [[CrossRef](#)]
22. Petersen, A.R.; Taylor, R.A.; Vicente-Hernández, I.; Mallender, P.R.; Olley, H.; White, A.J.P.; Britovsek, G.J.P. Oxygen Insertion into Metal Carbon Bonds: Formation of Methylperoxo Pd(II) and Pt(II) Complexes via Photogenerated Dinuclear Intermediates. *J. Am. Chem. Soc.* **2014**, *136*, 14089–14099. [[CrossRef](#)] [[PubMed](#)]
23. McGuire, R., Jr.; Clark McGuire, M.; McMillin, D.R. Platinum(II) polypyridines: A tale of two axes. *Coord. Chem. Rev.* **2010**, *254*, 2574–2583. [[CrossRef](#)]
24. Sakamoto, R.; Katagiri, S.; Maeda, H.; Nishihara, H. Bis(terpyridine) metal complex wires: Excellent long-range electron transfer ability and controllable intrawire redox conduction on silicon electrode. *Coord. Chem. Rev.* **2013**, *257*, 1493–1506. [[CrossRef](#)]
25. Hamacher, C.; Hurkes, N.; Kaiser, A.; Klein, A.; Schüren, A. On the Electrochemistry and Spectroscopy of Organometallic Terpyridine Nickel Complexes. *Inorg. Chem.* **2009**, *48*, 9947–9951. [[CrossRef](#)]
26. Cummings, S.D. Platinum complexes of terpyridine: Interaction and reactivity with biomolecules. *Coord. Chem. Rev.* **2009**, *253*, 1495–1516. [[CrossRef](#)]
27. Koizumi, T.-A.; Tomon, T.; Tanaka, K. Synthesis, Structures and Fluxional Behavior of Ruthenium(II) Complexes Bearing a Bidentate 1,8-Naphthyridine Ligand. *Bull. Chem. Soc. Jpn.* **2003**, *76*, 1969–1975. [[CrossRef](#)]
28. Kershaw Cook, L.J.; Halcrow, M.A. Doping ruthenium complexes into a molecular spin-crossover material. *Polyhedron* **2015**, *87*, 91–97. [[CrossRef](#)]
29. Zvirzdinaite, M.; Garbe, S.; Arefyeva, N.; Krause, M.; von der Stück, R.; Klein, A. Palladium(II) complexes of ambidentate and potentially cyclometalating 5-aryl-3-(2'-pyridyl)-1,2,4-triazine ligands. *Eur. J. Inorg. Chem.* **2017**, 2011–2022. [[CrossRef](#)]

30. Intille, G.M.; Pfluger, C.E.; Baker, W.A., Jr. Crystal and molecular structure of chloro(2,2',2''-terpyridine)palladium(II)chloride dihydrate, $C_{15}H_{15}Cl_2N_3O_2Pd$. *J. Cryst. Mol. Struct.* **1973**, *3*, 47–54. [[CrossRef](#)]
31. Maidich, L.; Pilo, M.I.; Rourke, J.P.; Clarkson, G.J.; Canu, P.; Stoccoro, S.; Zucca, A. Classical vs. Non-Classical Cyclometalated Pt(II) Complexes. *Molecules* **2022**, *27*, 7249. [[CrossRef](#)]
32. Nabavizadeh, S.M.; Molaee, H.; Haddadi, E.; Niroomand Hosseini, F.; Hoseini, S.J.; Abu-Omar, M.M. Tetranuclear rollover cyclometalated organoplatinum–rhenium compounds; C–I oxidative addition and C–C reductive elimination using a rollover cycloplatinated dimer. *Dalton Trans.* **2021**, *50*, 15015–15026. [[CrossRef](#)]
33. Becker, Y.; Schön, F.; Becker, S.; Sun, Y.; Thiel, W.R. Structure-dependent regioselectivity of a roll-over cyclopalladation occurring at 2,2'-bipyridine-type ligands. *J. Organomet. Chem.* **2021**, *940*, 121780. [[CrossRef](#)]
34. Tovar-Ramírez, M.E.; Ramírez-Zúniga, R.; Nicasio-Collazo, J.; Wrobel, K.; Alvarado-Rodríguez, J.G.; Wrobel, K.; Serrano, O. Rollover Cyclopalladation via Remote C–H Bond Activation of Br-Pyridinbenzothiazole: An Experimental Study. *Chem. Select* **2018**, *3*, 4133–4139. [[CrossRef](#)]
35. Haque, A.; Xu, L.; Al-Balushi, R.A.; Al-Suti, M.K.; Ilmi, R.; Guo, Z.; Khan, M.S.; Wong, W.-Y.; Raithby, P.R. Cyclometallated tridentate platinum(II) arylacetylide complexes: Old wine in new bottles. *Chem. Soc. Rev.* **2019**, *48*, 5547–5563. [[CrossRef](#)]
36. Koshevoy, I.O.; Krause, M.; Klein, A. Non-Covalent Intramolecular Interactions through Ligand-Design Promoting Efficient Luminescence from Transition Metal Complexes. *Coord. Chem. Rev.* **2020**, *405*, 213094. [[CrossRef](#)]
37. Cebrián, C.; Mauro, M. Recent advances in phosphorescent platinum complexes for organic light-emitting diodes. *Beilstein J. Org. Chem.* **2018**, *14*, 1459–1481. [[CrossRef](#)]
38. Williams, J.A.G. The coordination chemistry of dipyritylbenzene: N-deficient terpyridine or panacea for brightly luminescent metal complexes? *Chem. Soc. Rev.* **2009**, *38*, 1783–1801. [[CrossRef](#)]
39. Krause, M.; von der Stück, R.; Brünkink, D.; Buss, S.; Doltsinis, N.L.; Strassert, C.A.; Klein, A. Platinum and palladium complexes of tridentate $-C^{\wedge}N^{\wedge}N$ (phen-ide)-pyridine-thiazol ligands—A case study involving spectroelectrochemistry, photoluminescence spectroscopy and TD-DFT calculations. *Inorg. Chim. Acta* **2021**, *518*, 120093. [[CrossRef](#)]
40. Garoni, E.; Boixel, J.; Dorcet, V.; Roisnel, T.; Roberto, D.; Jacquemin, D.; Guerchais, V. Controlling the emission in flexibly-linked ($N^{\wedge}C^{\wedge}N$)platinum dyads. *Dalton Trans.* **2018**, *47*, 224–232. [[CrossRef](#)]
41. Schulze, B.; Friebe, C.; Jäger, M.; Görls, H.; Birkner, E.; Winter, A.; Schubert, U.S. Pt^{II} Phosphors with Click-Derived 1,2,3-Triazole-Containing Tridentate Chelates. *Organometallics* **2018**, *37*, 145–155. [[CrossRef](#)]
42. Li, K.; Tong, G.S.M.; Wan, Q.; Cheng, G.; Tong, W.-Y.; Ang, W.-H.; Kwong, W.-L.; Che, C.-M. Highly phosphorescent platinum(II) emitters: Photophysics, materials and biological application. *Chem. Sci.* **2016**, *7*, 1653–1673. [[CrossRef](#)] [[PubMed](#)]
43. Kletsch, L.; Jordan, R.; Köcher, A.S.; Buss, S.; Strassert, C.A.; Klein, A. Photoluminescence of Ni(II), Pd(II), and Pt(II) Complexes [M(Me₂dpb)Cl] Obtained from C–H Activation of 1,5-Di(2-pyridyl)-2,4-dimethylbenzene (Me₂dpbH). *Molecules* **2021**, *26*, 5051. [[CrossRef](#)]
44. Eskelinen, T.; Buss, S.; Petrovskii, S.K.; Grachova, E.V.; Krause, M.; Klein, A.; Strassert, C.A.; Koshevoy, I.O.; Hirva, P. Photophysics and Excited State Dynamics of Cyclometalated [M(C[∧]N[∧]N)(CN)] (M = Ni, Pd, Pt) Complexes: A Theoretical and Experimental Study. *Inorg. Chem.* **2021**, *60*, 8777–8789. [[CrossRef](#)] [[PubMed](#)]
45. Wong, Y.-S.; Tang, M.-C.; Ng, M.; Yam, V.W.-W. Toward the Design of Phosphorescent Emitters of Cyclometalated Earth-Abundant Nickel(II) and Their Supramolecular Study. *J. Am. Chem. Soc.* **2020**, *142*, 7638–7646. [[CrossRef](#)]
46. Cardenas, D.J.; Echavarren, A.M.; Ramirez de Arellano, M.C. Divergent Behavior of Palladium(II) and Platinum(II) in the Metalation of 1,3-Di(2-pyridyl)benzene. *Organometallics* **1999**, *18*, 3337–3341. [[CrossRef](#)]
47. Ogata, K.; Sasano, D.; Yokoi, T.; Isozaki, K.; Yoshida, R.; Takenaka, T.; Seike, H.; Ogawa, T.; Kurata, H.; Yasuda, N.; et al. Synthesis and Self-Assembly of NCN-Pincer Pd-Complex-Bound Norvalines. *Chem.–Eur. J.* **2013**, *19*, 12356–12375. [[CrossRef](#)]
48. Soro, B.; Stoccoro, S.; Minghetti, G.; Zucca, A.; Cinellu, M.A.; Manassero, M.; Gladiali, S. The first pincer-aryl [M–(NCN)] complexes [M = Pd(II); Pt(II)] with chiral pyridine donors: Synthesis and catalytic activity in C–C bond formation. *Inorg. Chim. Acta* **2006**, *359*, 1879–1888. [[CrossRef](#)]
49. Soro, B.; Stoccoro, S.; Minghetti, G.; Zucca, A.; Cinellu, M.A.; Gladiali, S.; Manassero, M.; Sansoni, M. Synthesis of the First C-2 Cyclopalladated Derivatives of 1,3-Bis(2-pyridyl)benzene. Crystal Structures of [Hg(N-C-N)Cl], [Pd(N-C-N)Cl], and [Pd₂(N-C-N)₂(μ-OAc)₂][Hg₂Cl₆]. Catalytic Activity in the Heck Reaction. *Organometallics* **2005**, *24*, 53–61. [[CrossRef](#)]
50. Kletsch, L.; Hörner, G.; Klein, A. Cyclometalated Ni(II) complexes [Ni(N[∧]C[∧]N)X] of the tridentate 2,6-di(2-pyridyl)-phen-ide ligand. *Organometallics* **2020**, *39*, 2820–2829. [[CrossRef](#)]
51. Vogt, N.; Sivchik, V.; Sandleben, A.; Hörner, G.; Klein, A. Direct Base-Assisted C–H Cyclonickelation of 6-Phenyl-2,2'-bipyridine. *Molecules* **2020**, *25*, 997. [[CrossRef](#)]
52. Vogt, N.; Sandleben, A.; Kletsch, L.; Schäfer, S.; Chin, M.T.; Vivic, D.A.; Hörner, G.; Klein, A. On the Role of the X Coligands in Cyclometalated [Ni(Phppy)X] Complexes (HPhppy = 6-phenyl-2,2'-bipyridine). *Organometallics* **2021**, *40*, 1776–1785. [[CrossRef](#)]
53. Mousa, A.H.; Chakrabarti, K.; Isapour, G.; Bendix, J.; Wendt, O.F. Enhancing the Stability of Aromatic PCN Pincer Nickel Complexes by Incorporation of Pyridine as the Nitrogen Side Arm. *Eur. J. Inorg. Chem.* **2020**, 4270–4277. [[CrossRef](#)]
54. Manfroni, G.; Capomolla, S.S.; Prescimone, A.; Constable, E.C.; Housecroft, C.E. Isomeric 4,2':6',4''- and 3,2':6',3''-Terpyridines with Isomeric 4'-Trifluoromethylphenyl Substituents: Effects on the Assembly of Coordination Polymers with [Cu(hfacac)₂] (Hhfacac = Hexafluoropentane-2,4-dione). *Inorganics* **2021**, *9*, 54. [[CrossRef](#)]

55. Rocco, D.; Novak, S.; Prescimone, A.; Constable, E.C.; Housecroft, C.E. Manipulating the Conformation of 3,2':6',3''-Terpyridine in $[\text{Cu}_2(\mu\text{-OAc})_4(3,2':6',3''\text{-tpy})_n]$ 1D-Polymers. *Chemistry* **2021**, *3*, 182–198. [[CrossRef](#)]
56. Feuerstein, W.; Breher, F. Synthetic access to a phosphorescent non-palindromic pincer complex of palladium by a double oxidative addition—comproportionation sequence. *Chem. Commun.* **2020**, *56*, 12589–12592. [[CrossRef](#)]
57. Okamura, T.-a.; Ishikawa, M.; Onitsuka, K. Unsymmetrical Metallosupramolecular Polycondensation of Expanded L-Amino Acid Containing Platinum(II) Complex in Nonpolar Solvents. *ACS Appl. Polym. Mater.* **2022**, *4*, 9472–9481. [[CrossRef](#)]
58. Zhang, Q.; Wang, S.; Zhu, Y.; Zhang, C.; Cao, H.; Ma, W.; Tian, X.; Wu, J.; Zhou, H.; Tian, Y. Functional Platinum(II) Complexes with Four-Photon Absorption Activity, Lysosome Specificity, and Precise Cancer Therapy. *Inorg. Chem.* **2021**, *60*, 2362–2371. [[CrossRef](#)]
59. Ranieri, A.M.; Vezzelli, M.; Leslie, K.G.; Huang, S.; Stagni, S.; Jacquemin, D.; Jiang, H.; Hubbard, A.; Rigamonti, L.; Watkin, E.L.J.; et al. Structure illumination microscopy imaging of lipid vesicles in live bacteria with naphthalimide appended organometallic complexes. *Analyst* **2021**, *146*, 3818–3822. [[CrossRef](#)]
60. Garbe, S.; Krause, M.; Klimpel, A.; Neundorff, I.; Lippmann, P.; Ott, I.; Brünkink, D.; Strassert, C.A.; Doltsinis, N.L.; Klein, A. Cyclometalated Pt Complexes of CNC Pincer Ligands: Luminescence and Cytotoxic Evaluation. *Organometallics* **2020**, *39*, 746–756. [[CrossRef](#)]
61. Kergreis, A.; Lord, R.M.; Pike, S.J. Influence of Ligand and Nuclearity on the Cytotoxicity of Cyclometallated C^NC Platinum(II) Complexes. *Chem.–Eur. J.* **2020**, *26*, 14938–14946. [[CrossRef](#)] [[PubMed](#)]
62. Hamidzadeh, P.; Nabavizadeh, S.M.; Hoseini, S.J. Effects of the number of cyclometalated rings and ancillary ligands on the rate of MeI oxidative addition to platinum(II)–pincer complexes. *Dalton Trans.* **2019**, *48*, 3422–3432. [[CrossRef](#)]
63. Campillo, D.; Escudero, D.; Baya, M.; Martín, A. Heteropolymetallic Architectures as Snapshots of Transmetallation Processes at Different Degrees of Transfer. *Chem.–Eur. J.* **2022**, *28*, e202104538. [[CrossRef](#)] [[PubMed](#)]
64. Niazi, M.; Klein, A. DFT Investigation of the Molecular Properties of the Dimethylglyoximato Complexes $[\text{M}(\text{Hdmg})_2]$ (M = Ni, Pd, Pt). *Inorganics* **2021**, *9*, 47. [[CrossRef](#)]
65. Haseloer, A.; Jordan, R.; Denkler, L.M.; Reimer, M.; Olthof, S.; Schmidt, I.; Meerholz, K.; Hörner, G.; Klein, A. Ni, Pd, and Pt complexes of a tetradentate dianionic thiosemicarbazone-based O^NN^S ligand. *Dalton Trans.* **2021**, *50*, 4311–4322. [[CrossRef](#)]
66. Kröhnke, F. The Specific Synthesis of Pyridines and Oligopyridines. *Synthesis* **1976**, *1976*, 1–24. [[CrossRef](#)]
67. Lai, S.-W.; Cheung, T.-C.; Chan, M.C.W.; Cheung, K.-K.; Peng, S.-M.; Che, C.-M. Luminescent Mononuclear and Binuclear Cyclometalated Palladium(II) Complexes of 6-Phenyl-2,2'-bipyridines: Spectroscopic and Structural Comparisons with Platinum(II) Analogues. *Inorg. Chem.* **2000**, *39*, 255–262. [[CrossRef](#)]
68. Janzen, D.E.; Mann, K.R. Red and Orange Polymorphs of $[\text{Pt}(\text{terpy})\text{Cl}]\text{Cl}\cdot 2\text{H}_2\text{O}$. *J. Chem. Crystallogr.* **2013**, *43*, 292–298. [[CrossRef](#)]
69. Deka, R.; Sarkar, A.; Butcher, R.J.; Junk, P.C.; Turner, D.R.; Deacon, G.B.; Singh, H.B. Isolation of Homoleptic Dicationic Tellurium and Monocationic Bismuth Analogues of Non-N-Heterocyclic Carbene Derivatives. *Organometallics* **2020**, *39*, 334–343. [[CrossRef](#)]
70. Bercaw, J.E.; Durrell, A.C.; Gray, H.B.; Green, J.C.; Hazari, N.; Labinger, J.A.; Winkler, J.R. Electronic Structures of Pd^{II} Dimers. *Inorg. Chem.* **2010**, *49*, 1801–1810. [[CrossRef](#)]
71. Niedzielska, D.; Pawlak, T.; Wojtczak, A.; Pazderski, L.; Szlyk, E. Structural and ¹H, ¹³C, ¹⁵N NMR spectroscopic studies of Pd(II) chloride organometallics with 2-phenylpyridine and ammonia, pyridine or its methyl derivatives. *Polyhedron* **2015**, *92*, 41–51. [[CrossRef](#)]
72. Kim, Y.-J.; Chang, X.; Han, J.-T.K.; Lim, M.S.; Lee, S.W. Cyclometallated Pd(II) azido complexes containing 6-phenyl-2,2'-bipyridyl or 2-phenylpyridyl derivatives: Synthesis and reactivity toward organic isocyanides and isothiocyanates. *Dalton Trans.* **2004**, *21*, 3699–3708. [[CrossRef](#)]
73. Williams, J.A.G.; Beeby, A.; Davies, E.S.; Weinstein, J.A.; Wilson, C. An Alternative Route to Highly Luminescent Platinum(II) Complexes: Cyclometalation with N^CN-Coordinating Dipyridylbenzene Ligands. *Inorg. Chem.* **2003**, *42*, 8609–8611. [[CrossRef](#)]
74. Poirier, S.; Lynn, H.; Reber, C.; Tailleur, E.; Marchivie, M.; Guionneau, P.; Probert, M.R. Variation of M⋯H–C Interactions in Square-Planar Complexes of Nickel(II), Palladium(II), and Platinum(II) Probed by Luminescence Spectroscopy and X-ray Diffraction at Variable Pressure. *Inorg. Chem.* **2018**, *57*, 7713–7723. [[CrossRef](#)]
75. Wang, Z.; Turner, E.; Mahoney, V.; Madakuni, S.; Groy, T.; Li, J. Facile Synthesis and Characterization of Phosphorescent Pt(N^CN)X Complexes. *Inorg. Chem.* **2010**, *49*, 11276–11286. [[CrossRef](#)]
76. Chen, Y.; Li, K.; Lu, W.; Chui, S.S.-Y.; Ma, C.-W.; Che, C.-M. Photoresponsive Supramolecular Organometallic Nanosheets Induced by Pt^{II}⋯Pt^{II} and C–H⋯π Interactions. *Angew. Chem. Int. Ed.* **2009**, *48*, 9909–9913. [[CrossRef](#)]
77. APEX3—Software Suite for Crystallographic Programs, Bruker AXS, Inc.: Madison, WI, USA, 2015.
78. Sheldrick, G.M. Crystal Structure Refinement with SHELXL. *Acta Crystallogr. Sect. C Struct. Chem.* **2015**, *71*, 3–8. [[CrossRef](#)]
79. Sheldrick, G.M. A short history of SHELX. *Acta Crystallogr. Sect. A Found. Crystallogr.* **2008**, *64*, 112–122. [[CrossRef](#)]

Disclaimer/Publisher's Note: The statements, opinions and data contained in all publications are solely those of the individual author(s) and contributor(s) and not of MDPI and/or the editor(s). MDPI and/or the editor(s) disclaim responsibility for any injury to people or property resulting from any ideas, methods, instructions or products referred to in the content.